Tetralogy of Fallot

R. W. Sprengers, A. A. W. Roest, and L. J. M. Kroft

Contents

1 Introduction

Tetralogy of Fallot (TOF) is the most common of cyanotic congenital heart diseases. In this chapter essential background information regarding etiology, clinical presentation, and treatment options in TOF are presented. The main focus is on imaging adult TOF, discussing the full spectrum of image modalities with special attention for CT and MRI. Findings in TOF, late outcome aspects, follow-up of complications, and the role of imaging in guiding therapy are discussed.

1.1 Etiology

Tetralogy of Fallot (TOF) is named after Étienne-Louis Arthur Fallot, who refined earlier descriptions of the condition in his work "L'anatomie pathologique de la maladie bleu." TOF classically consists of a tetrad of (1) right ventricular outflow tract obstruction, (2) ventricular septal defect (VSD), (3) misalignment (dextroposition, also referred to as "overriding") of the aorta, and (4) right ventricular hypertrophy (Fig. 1).

The key pathological components in TOF are anterocephalad deviation of the insertion of the outflow septum and hypertrophy of the septoparietal trabeculations of the right ventricular outflow tract, resulting in pulmonary stenosis. The anterocephalad deviation of the outflow septum results in an interventricular communication (VSD) in continuity with the aortic valve (Pacheco Duro et al. 2010).

R. W. Sprengers • L. J. M. Kroft (✉)
Department of Radiology, Leiden University Medical Center, Postbus 9600, 2300 RC, Leiden, The Netherlands
e-mail: L.J.M.Kroft@lumc.nl

A. A. W. Roest
Department of Pediatric Cardiology, Leiden University Medical Center, Leiden, The Netherlands

Med Radiol Diagn Imaging (2017)
DOI 10.1007/174_2017_107, © Springer International Publishing AG
Published Online: 13 July 2017

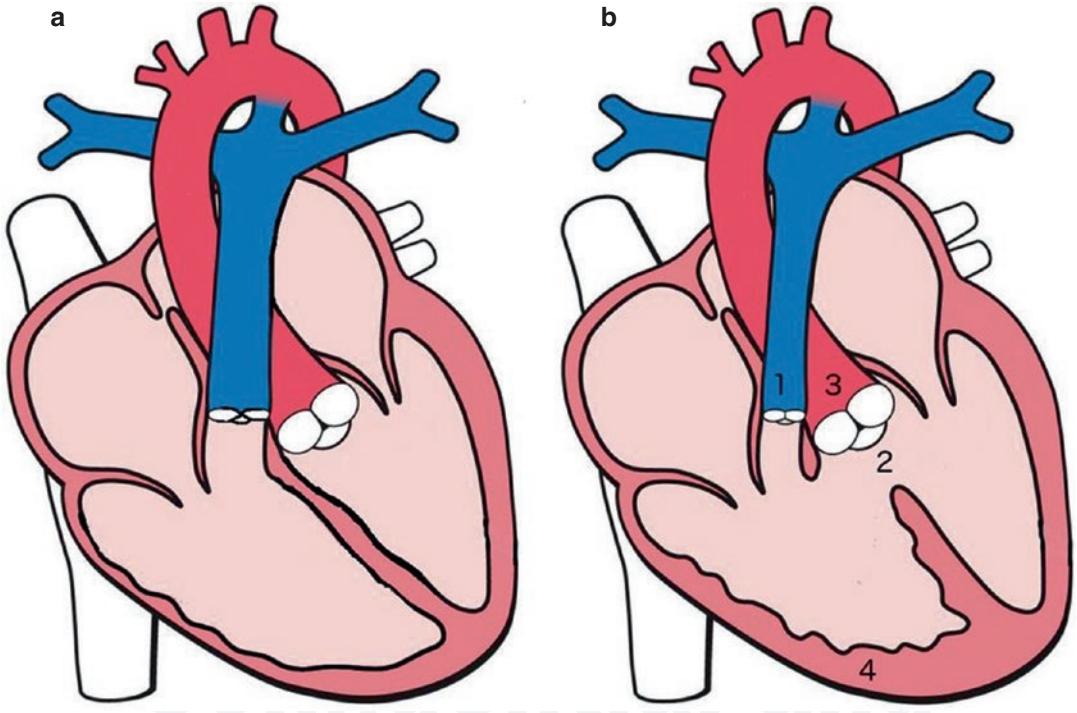

Fig. 1 (**a**) Schematic drawing of a normal heart. (**b**) Schematic drawing of the tetralogy of Fallot. Tetralogy of Fallot consists of (*1*) right ventricular outflow tract obstruction, (*2*) a ventricular septum defect, (*3*) overriding of the aorta over the interventricular septum, and (*4*) right ventricular hypertrophy. Drawing adapted from www.obgenkey.com

The aortic valve thus has a biventricular connection and the degree to which the aortic valve is positioned above the right ventricle is referred to as the degree of "overriding." Misalignment between the outflow septum and the septoparietal trabeculations leads to hypertrophy of the latter and subsequently results in pulmonary valve stenosis or infundibular stenosis. TOF with pulmonary atresia is a severe variant with complete obstruction of the right ventricular outflow tract and agenesis of the pulmonary trunk. The forth feature of the tetrad, right ventricular hypertrophy, is a hemodynamic consequence of the anatomical anomalies.

In addition to the tetrad described above, TOF is associated with a variety of other anomalies, including a bicuspid pulmonary valve, stenosis of the left pulmonary artery, dextroposition of the aortic arch, a patent oval foramen or atrial septal defect (ASD) (also referred to as the pentalogy of Fallot), an atrioventricular septum defect (AVSD) and anomalous pulmonary venous return.

1.2 Clinical Presentation

Fetal circulation is not affected by TOF. After birth however, the lungs replace placental blood oxygenation; adequate blood flow to the lungs is essential. TOF results in lower levels of oxygenated blood due to the right-to-left shunt of deoxygenated blood from the right ventricle through the VSD. The VSD is usually large, and in combination with the right ventricular outflow obstruction, results in equal pressure in both ventricles. Because of the right ventricular outflow tract obstruction preferential blood flow from both ventricles is through the aortic valve, resulting in a right-to-left shunt and cyanosis (Sommer et al. 2008). However, in case of mild outflow tract obstruction this shunt may be small, and sufficient blood flow to the lungs results in normal levels of oxygenation (non-cyanotic or "pink" Fallot).

TOF is frequently diagnosed during fetal life, but most patients present in the first months after

birth (Apitz et al. 2009). The primary symptom is low blood oxygenation resulting in failure to thrive, dyspnea, and cyanosis. The severity of symptoms is determined by the amount of pulmonary blood flow, which is influenced by the functional behavior of the right ventricular outflow tract obstruction, and physiological aspects such as ventricular and systemic arterial pressures and the origin of pulmonary blood flow (i.e., coming from the right ventricle, or through the ductus arteriosus or collateral arteries from the aorta or bronchopulmonary arteries). Most patients have adequate pulmonary blood flow at birth and become cyanotic weeks to months after birth, due to progressive outflow tract stenosis and right-to-left shunting. However, if blood oxygenation is severely hampered after birth, patients present with cyanosis immediately.

A particular presentation of TOF are recurrent hypercyanotic spells, presumably caused by transient increased pulmonary blood flow resistance or contraction of the right ventricular infundibulum, resulting in increased preferential flow of deoxygenated blood to the systemic circulation. This results in sudden onset of (increased) cyanosis and may lead to syncope, hypoxic injury, and death.

1.3 Current Treatment Options

Before surgical intervention was introduced about 35% of the patients with TOF died within the first year of life, 50% reached the age of 3 years, and survival after the age of 30 years was exceptional (Bertranou et al. 1978). Nowadays, almost all patients that receive surgical correction can expect to reach adult life. Corrective surgery aims to completely close the VSD and create an unobstructed ventricular outflow tract, with preservation of the right ventricular function and pulmonary valve function. In the early years of corrective surgery, repair was performed by means of right ventriculotomy. From the mid sixties transatrial-transpulmonary approaches with or without patch repair of the outflow tract improved early to middle-term outcome (Karl et al. 1992). Currently, correction of TOF has evolved from complete relief of outflow obstruction with extensive resection of infundibular muscles, often at the expense of pulmonary valve regurgitation, towards accepting residual obstruction in order to preserve pulmonary valve function, with the aim to minimize late adverse effects (Van Arsdell et al. 2005).

The best age for elective surgical repair is now considered to be within the first year of life (Van Arsdell et al. 2000; Al Habib et al. 2010). Surgical repair in patients younger than 3 months has been associated with extended intensive care stay and hospitalization (Van Arsdell et al. 2000). Many centers reserve such early repair for patients presenting with severe cyanosis or hypercyanotic spells. Potential disadvantages of surgical correction later in life include complications of long-lasting right ventricle pressure overload and cardiomyopathy due to long-term hypoxemia, which has been related to ventricular dysfunction and arrhythmias (Chowdhury et al. 2006).

In patients who are not fit for primary corrective surgery (contraindications include aberrant coronary arteries, small caliber pulmonary arteries, and coexisting cardiac malformations) palliative surgery is performed. The goal of palliative surgery is to increase the pulmonary blood flow and/or to create a time-window as to allow pulmonary arteries to grow in preparation for corrective repair at second stage. Various types of palliative procedures have been developed over time, but have also been abandoned because of complications or imposing difficulties on secondary corrective procedures. The current palliative surgery procedure of choice is the modified Blalock-Taussig shunt, where a Gore-Tex graft is placed between one of the arch vessels and the pulmonary artery. This shunt increases pulmonary blood flow and helps the pulmonary arteries to develop (Jahangiri et al. 1999). The risk of complications related to the arch vessel is small.

1.4 Complications and Treatment Options

Most corrective surgery procedures have an uncomplicated course. A minority of infants develops a low cardiac output syndrome or junctional

ectopic tachycardia (Cullen et al. 1995; Tharakan et al. 2014). These conditions are presumably caused by mechanical trauma to the myocardium or the conductive tissue and are of a transient nature, but require prolonged and intensive care.

Some TOF patients may have major aortopulmonary collateral arteries (MACPAs). MAPCAs are intersegmental arteries arising at various points from the descending aorta that connect to the pulmonary hilum to supply the lungs with blood. With normal development of the pulmonary arteries these connections regress during embryogenesis, but MAPCAs may persist in case of pulmonary atresia (Boshoff et al. 2006). Because of their similar anatomy MAPCAs are likely dilated bronchial arteries (Nørgaard et al. 2006). MAPCAs increase in size with physical growth and large MAPCAs may lead to pulmonary hypertension, often necessitating intervention early in life (Prieto 2005). MAPCAs may further lead to compression of the esophagus and airways. Importantly, MAPCAs may cause major and fatal bleeding (Miyazaki et al. 2001; Lanjewar et al. 2012; Sharma et al. 2016).

The majority of late complications is related to pulmonary valve regurgitation and are major cause of reoperation. Other complications include aortic root dilatation, regurgitation of the tricuspid and aortic valve, and shunt-related complication after palliative surgery.

Previously, surgery focused on complete relief of right ventricular outflow tract obstruction, accepting freely regurgitant pulmonary flow and dilatation of the outflow tract. However, the degree of pulmonary valve regurgitation has now been related to adverse late outcomes, including biventricular heart failure, ventricular arrhythmia, and sudden death. Imaging plays an essential role in the evaluation and follow-up of TOF patients.

2 Imaging Goals

The natural course of pulmonary valve regurgitation is slow and late adverse effects usually present only after decades. Although complications can occur at young age, they are few during the first 30 years of life. Older patients with important pulmonary valve regurgitation may rapidly develop progressive and fatal right ventricular failure (Shimazaki et al. 1984). Studies have demonstrated a direct relation between the severity of pulmonary valve regurgitation and right ventricular dilatation (Carvalho et al. 1992; Rebergen et al. 1993). Pulmonary valve regurgitation also relates to right ventricular afterload that is increased in patients with coexisting pulmonary artery stenosis (Chaturvedi et al. 1997). Moreover, a multicenter study in almost 800 patients has demonstrated that pulmonary valve regurgitation is an important determinant of symptomatic ventricular arrhythmia (Berul et al. 1997). Imaging plays an important part in the follow-up of patients with TOF and mainly focuses on the assessment of pulmonary valve regurgitation and right ventricular dilatation. With quantifying changes in pulmonary valve regurgitation and right ventricular dilatation over time, imaging assists in decision-making and timing pulmonary valve replacement. Optimal timing of pulmonary valve replacement is a topic of ongoing research.

Furthermore, imaging is used for the assessment of coexisting abnormalities and other late-term complications, such as aortic root dilatation. Progressive aortic valve regurgitation and a root diameter over 55 mm are commonly accepted as indication for aortic root surgery, especially when an indication for pulmonary valve replacement already exists (Apitz et al. 2009). In addition, with increasing survival, late adult life conditions such as atherosclerotic coronary artery disease are new aspects in the management of (older) TOF patients (Coutu et al. 2004). Imaging assists in early detection and therapy guidance (e.g., preoperative surgical revascularization assessment).

Various imaging modalities are involved in the assessment of TOF patients, each with specific aims and/or possibilities. The role of echocardiography, conventional X-ray, CT and MR techniques and nuclear imaging will be discussed below.

3 Imaging Techniques

3.1 Echocardiography

Echocardiography provides real-time assessment of ventricular size and function, myocardial wall thickness and motion, valvular anatomy and

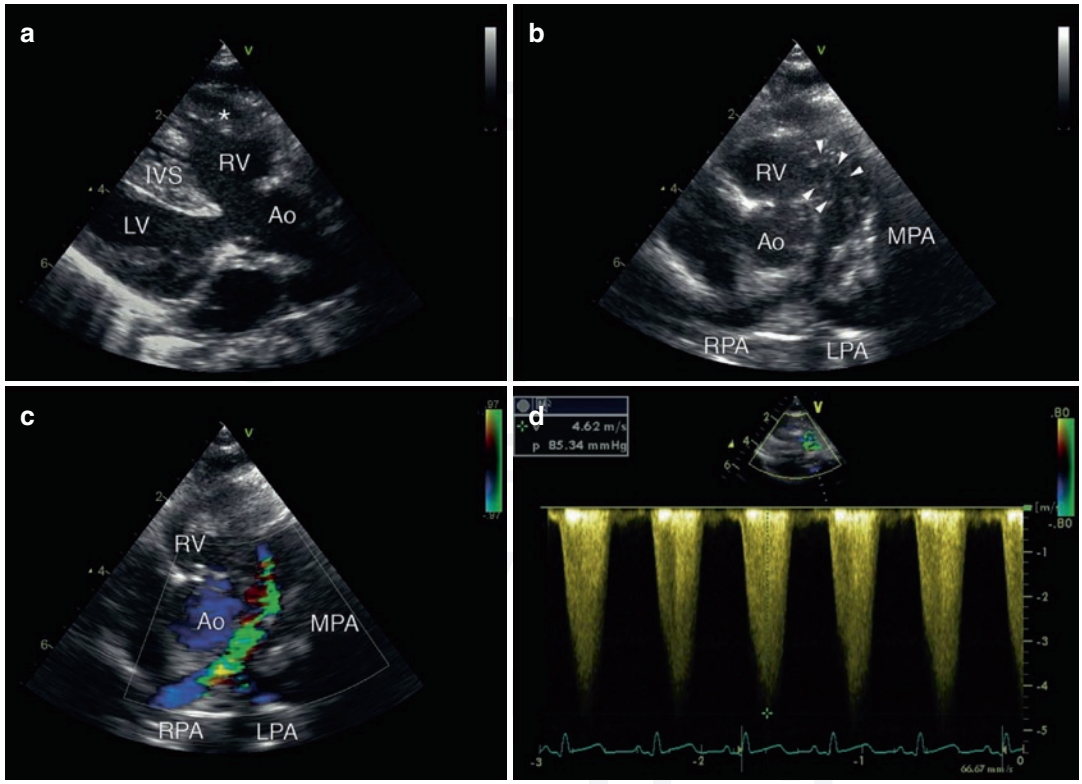

Fig. 2 Two-month-old female patient with uncorrected tetralogy of Fallot. Using echocardiography with 2D grey-scale imaging the tetrad of abnormalities can be evaluated (**a**, **b**): overriding of the aorta (Ao) over the interventricular septum (IVS), with subsequent ventricular septal defect, hypertrophy of the right ventricle (RV, *asterisk*) and narrowing of the right ventricular outflow tract (*arrowheads*). Using 2D color Doppler echocardiography (**c**) turbulence starting in the right ventricular outflow tract and continuing in the main pulmonary artery (MPA) can be seen. Continuous wave Doppler measurements (**d**) allow the evaluation of the pressure gradient over the right ventricular outflow tract and the MPA, with the use of the modified Bernouilli equation. Maximum velocity was 4.6 m/s, corresponding to a pressure gradient of 85 mmHg (*LV* left ventricle, *RPA* right pulmonary artery, *LPA* left pulmonary artery)

function, and hemodynamic information. It is readily available, non-invasive, fast, and inexpensive. Echocardiography plays a crucial role during fetal life and in small children with TOF (Fig. 2), as well as during early follow-up after corrective surgery. Over time, increasing emphasis is put towards recognizing pulmonary valve regurgitation and right ventricular dysfunction. Objective, reliable, and repeatable measurements for right ventricular size and function and pulmonary valve regurgitation are needed to guide future follow-up and therapy. Children can be evaluated well with echocardiography; however, imaging in adults may become limited by restricted acoustic window (Valente et al. 2014).

Quantitative functional analysis of the right ventricle encompasses both geometrical measurement of the volume, and nongeometrical parameters including TAPSE (tricuspid annular plane systolic excursion) and Doppler studies. The right ventricular volume and function can be derived from 2D echocardiographic measurements, using methods like the RVOT fractional shortening and the fractional area change. These parameters can be readily acquired. However, calculation of the right ventricular ejection fraction from the fractional area change is suboptimal because the calculation assumes a conical ventricular shape. Although applicable for the left ventricle, it is not for the right ventricle, in particular not in TOF patients with surgically corrected RVOT and right ventricular dilatation, especially at the apical level (Van der Hulst et al. 2011; Carminati et al. 2015). Three-dimensional (3D)

echocardiography may improve right ventricular evaluation but is still hampered by limited spatial and temporal resolution. 3D echocardiography underestimates the right ventricular volume and function, especially in larger right ventricles (with an end-diastolic volume over 200 mL), which is often the case in TOF patients (Iriart et al. 2009; Khoo et al. 2009; Shimada et al. 2010).

TAPSE measures the systolic displacement of the annular plane towards the ventricular apex and is widely used as an indicator for right ventricular function in the general population. However, the longitudinal shortening of the right ventricle is measured only while contractions may be dominant in other directions, especially in ventricular hypertrophy. A study in TOF patients has shown weak correlation between TAPSE and right ventricular function (i.e., ejection fraction) (Koestenberger et al. 2011).

Doppler echocardiography delivers hemodynamic information, such as measurement of the pulmonary gradient, which can help in decision-making for pulmonary valve replacement (Carminati et al. 2015).

Thus, although echocardiography is readily available and widely used as the primary imaging modality for follow-up TOF patients after corrective surgery, the reliability and repeatability specifically for right ventricular measures is limited (Carminati et al. 2015). Follow-up of adult TOF patients is therefore often complimented with other imaging modalities, especially when echocardiographic findings indicate deteriorating right ventricular function. The current guidelines for the management of adults with congenital heart disease recommend annual 2D echocardiography, complimented with cardiac MRI every 2–3 years (Warnes et al. 2008).

3.2 Radiography

Chest radiographs in patients with TOF may classically demonstrate a boot-shaped appearance of the heart (Fig. 3). Right ventricular hypertrophy may elevate the left ventricular apex, resulting in the upturned appearance of the heart. A small main pulmonary artery may further result in a narrow mediastinum, the "upper part of the boot." The upturning of the heart apex increases with the severity of RVOT obstruction. Although it is said to be classic, only infants with severe TOF demonstrate the sign (Haider 2008). Historically, the sign could be seen in older patients too, demonstrated by an old study in patients aged 14 weeks to 32 years, showing the boot-shaped heart sign in up to 70% of cases (Johnson 1965). Because the diagnosis of congenital heart disease is currently usually made early in (prenatal) life by echocardiography and followed by treatment within the first year of life, the sign is now only seen in infants with severe pulmonary atresia or older patients who have not been treated. Noteworthy, a frontal chest radiograph of a normal heart with a lordotic projection may result in a "false-positive" boot-shaped heart sign as well.

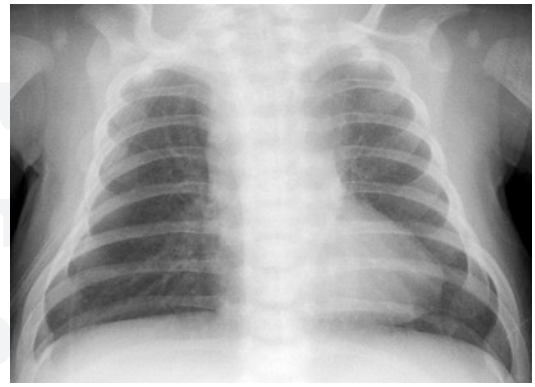

Fig. 3 Six-week-old female patient with uncorrected TOF. Frontal chest X-ray taken preoperatively, showing a boot-shaped appearance of the heart with elevated left ventricular apex

The role of chest radiographs in the follow-up of adults with TOF is limited. The anteriorly located right ventricle occupies little of the cardiac silhouette; chest radiographs have therefore low sensitivity in the evaluation of right ventricular failure (Boxt 1999). Also, indirect signs of deteriorating right ventricular function (e.g., changes in pulmonary circulation) cannot be depicted well enough, and chest radiographs are insufficient to guide follow-up or therapy. However, chest radiographs may be useful for the detection of stent fractures in patients with valve-containing pulmonary artery stent grafts (McElhinney 2011) (Fig. 4).

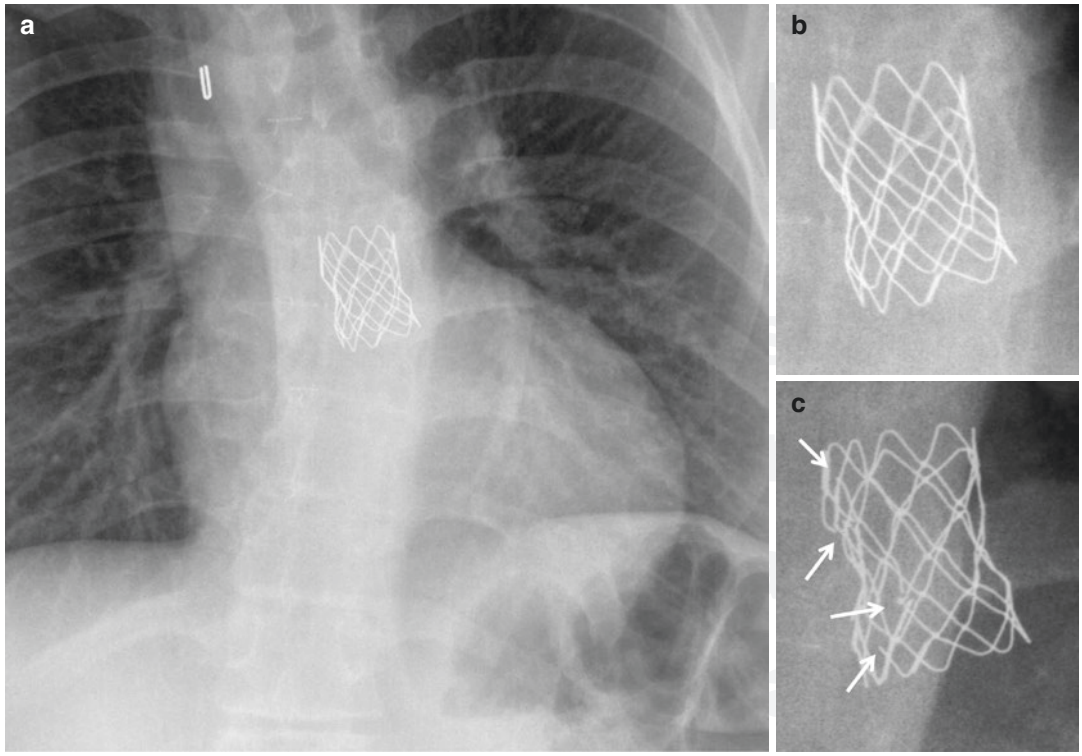

Fig. 4 Twelve-year-old female patient with corrected TOF after pulmonary valve replacement with a valve-containing stent graft. Frontal chest X-ray (**a**) and detailed views (**b**, **c**). Suboptimal deployment of the stent graft with slight residual stenosis at the level of the pulmonary valve (**a**, **b**). Approximately 6 months later (**c**): multiple stent-strut fractures (*arrows*) with signs of progressive stenosis

3.3 CT

Advances in multidetector row computed tomography (CT) technology have resulted in increased spatial and temporal resolution. New reconstruction algorithms allow improved image quality with a substantial reduction in ionizing radiation dose. The improvements in temporal resolution have also greatly boosted the application of CT for cardiac imaging, nowadays allowing for imaging of the whole heart in a single breath-hold, or even in a fraction of a second.

Because CT images are reconstructed from multiple projections, CT is sensitive to motion that result in blurring artifacts. To reduce motion artifacts, data acquisition is performed during breath-hold (minimizing respiration related motion artifacts) and prospective ECG triggering. ECG triggering is used to time data acquisition during the rest phase of the cardiac cycle, when motion of the heart itself is at minimum. In patients with slow heart rates (e.g., <65 bpm), this is at mid-diastole. In patients with higher heart rates (e.g., >75 bpm), the mid-diastolic rest phase becomes too short and the best phase shifts to the end-systolic phase of the RR-interval. A slow heart rate improves image quality. For certain indications (e.g., coronary artery CT angiography) pharmacological heart rate control is usually indicated and beta-blockers are generally used. For selective indications imaging may be performed using retrospective ECG gating, where data is acquired during the full cardiac cycle (RR-interval) at the expense of higher radiation dose. Specific phases can then be retrospectively selected throughout the RR-interval. Also, the dataset can be reconstructed as a "movie-loop," for ventricular function analysis.

3.3.1 Ventricular Volume and Function

Right and left ventricular volumes and function can be determined with CT by using retrospective ECG reconstruction when acquired throughout

the cardiac cycle. Acquisition must include the end-systolic and end-diastolic phases. Multiple phases of the RR-interval are reconstructed with a 5 or 10% interval that can be displayed as movie-loop. A 10% interval is sufficient for global function analysis with reduced post-processing time and data transfer (Joemai et al. 2008). Global and regional function such as motion and wall thickening can be visually evaluated. End-diastolic volume, end-systolic volume, stroke volume, and ejection fraction can be (automatically) calculated after (automatically) drawing endocardial contours on the end-diastolic and end-systolic phases (Fig. 5 shows an example of left ventricular volume analysis). By drawing epicardial contours, ventricular mass can be calculated as well. CT

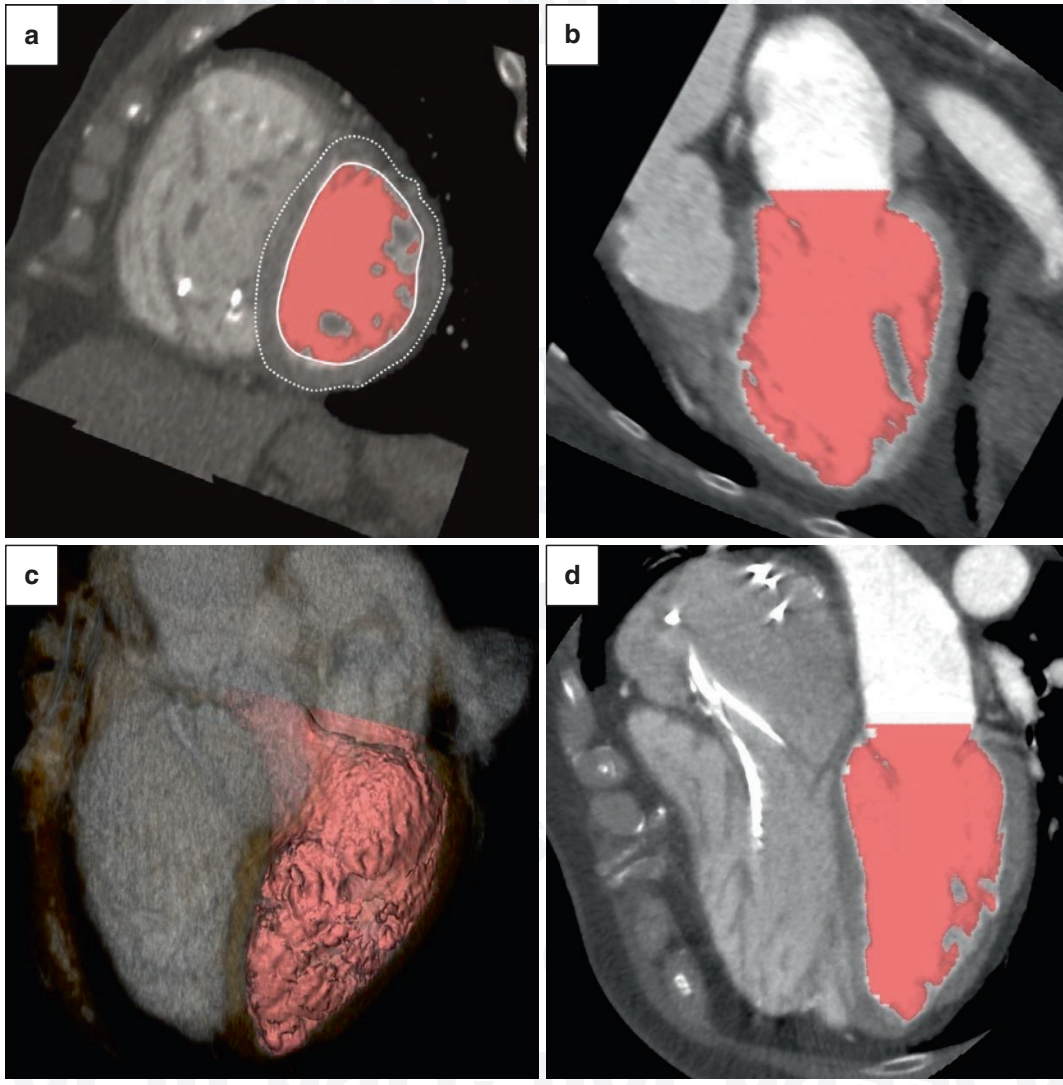

Fig. 5 Fifty-nine-year-old female patient with corrected TOF. CT views of the left ventricle in short axis (**a**), vertical long axis (**b**, **d**), and volume rendering (**c**). Automated detection of endocardial (continuous *line*) and epicardial (*dotted line*) contours of the left ventricle (**a**).The ventricular volume is automatically segmented (shaded areas in **a**, **b**, **c,** and **d**), with exclusion of the papillary muscles. This is automatically performed for all available phases throughout the cardiac cycle, including end-diastolic (**b**) and end-systolic phase (**d**). The end-diastolic volume, end-systolic volume, stroke volume, and ejection fraction are automatically calculated. The myocardial mass can be calculated from the difference between the endocardial volume from the epicardial volume. A volume rendering of the segmented volume (**c**) aids visual assessment of the ventricular function during playback of the "movie-loop." Note the pacemaker leads visible in the right atrium and ventricle in the end-systolic phase (**d**)

measurements of ventricular volume and function correlate well with cardiac MRI (Lembcke et al. 2005; Raman et al. 2006). Because of inherit radiation exposure, ventricular function assessment with cardiac CT should be reserved for patients with contraindications for cardiac MRI (see paragraph on MRI limitations).

3.3.2 Pulmonary Arteries

Because of its excellent spatial resolution, CT is an excellent tool for imaging the pulmonary arteries. Congenital abnormalities such as pulmonary artery stenosis and morphologic abnormalities after palliative surgical correction are often seen. With multiplanar reconstruction tools, CT provides an easy way to evaluate the pulmonary artery diameter or to visualize abnormal pulmonary artery course (Fig. 6).

CT allows for detailed imaging of the extent and course of MAPCAs (Fig. 7), often necessary before treatment.

Treatment of pulmonary artery stenosis is increasingly performed by means of balloon angioplasty and stenting (Fig. 8). The effects of treatment and complications such as intimal hyperplasia or stent fracture may be evaluated with CT.

3.3.3 Aortic Root

TOF may be complicated by aortic root dilatation. Both cardiac MRI and CT can be used to assess aortic dimensions. CT acquisition must be performed with ECG gating to prevent motion artifacts. Measurements should be performed in double oblique fashion (perpendicular to the axis of blood flow) and include the vessel wall for reproducibility and comparison reasons (Hiratzka et al. 2010). The topic aortic root dilatation is further discussed in the MRI section of this chapter.

3.3.4 Coronary Arteries

The role of CT in the assessment of atherosclerotic coronary artery disease and related risk stratification is well established. Increasing number of TOF patients reach age where atherosclerotic coronary artery disease may become relevant. Assessment of coronary artery disease in TOF patients is similar to any other patient. Preoperative

Fig. 7 Four-month-old male patient with pulmonary atresia. CT parasagittal view shows a major aortopulmonary collateral artery (MAPCA), arising from the descending aorta and connecting to the right hilum

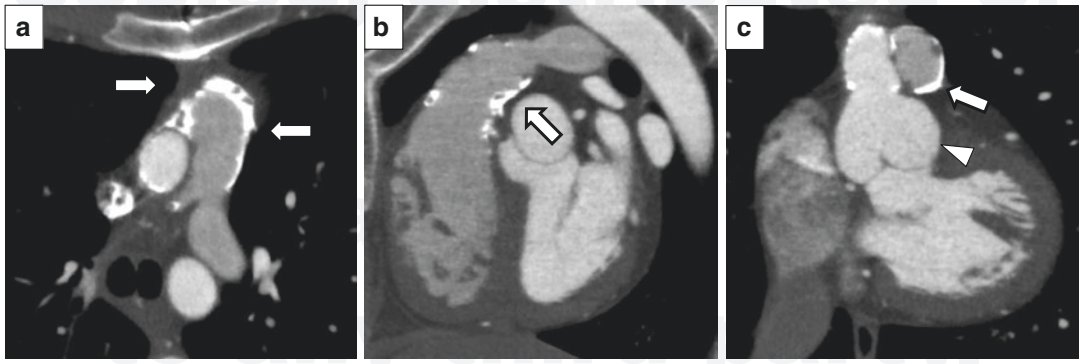

Fig. 6 Twenty-one-year-old male patient with a homograft conduit between the right ventricle and pulmonary arteries. CT multiplanar reconstruction (MPR) centered on the conduit with axial oblique (**a**), parasagittal (**b**), and double oblique semi-coronal view (**c**). MPR provides an easy way to evaluate the pulmonary artery diameter. Note the extensive calcifications in the RVOT and homograft (*arrows*), as well as a dilated aortic root (*arrowhead*)

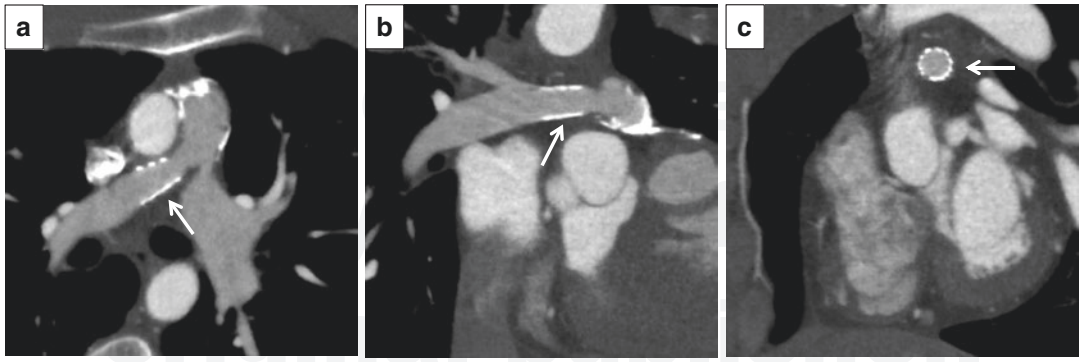

Fig. 8 Twenty-one-year-old male patient with corrected pulmonary atresia and right pulmonary artery stenosis. CT multiplanar reconstruction centered on the right pulmonary artery with axial oblique (**a**), coronal oblique (**b**), and double oblique view (**c**), showing a stent placed in the right pulmonary artery to treat the stenosis (*arrows*). The stent is well deployed without signs of restenosis or in-stent stenosis. The effects of treatment and the presence of complications can be easily evaluated with CT

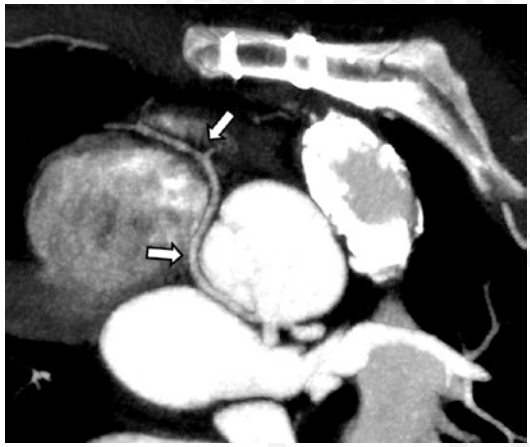

Fig. 9 Same patient as in Fig. 8. CT angiography with maximum intensity projection (MIP) of the coronary arteries, demonstrating an aberrant course of the right coronary artery (*arrows*) arising from the left coronary sinus with retro-aortic course to the right atrioventricular groove. A retro-aortic course is benign

assessment of the coronary artery anatomy in TOF patients, e.g., before (percutaneous) pulmonary valve implantation, may be performed by cardiac CT or MRI. Despite advances in cardiac MRI that improved the visualization of the coronary arteries, CT has much higher diagnostic accuracy (Hamdan et al. 2011). If evaluation of the origin or proximal course of the coronaries is uncertain on cardiac MRI, additional assessment with cardiac CT may be needed for planning surgical or percutaneous interventions (Fig. 9).

3.3.5 CT Limitations

The use of ionizing radiation is a drawback of CT. Since the risk for cancer increases with dose and repeated exposure, this is particularly true for follow-up (Brenner et al. 2003). Risks related to the administration of iodinated contrast agent are contrast-induced nephropathy and risk for allergic reaction (Weisbord et al. 2008; Andreucci et al. 2014).

3.4 MRI

Cardiac MRI is the imaging modality of first choice in adult TOF patients for follow-up and for assessing complications. Cardiovascular anatomy, biventricular size and function, myocardial viability, and blood flow and function can be evaluated. MRI is considered the reference standard for quantification of right ventricular size and function and pulmonary regurgitation (Kilner et al. 2010). Using an imaging protocol that combines multiple MRI techniques, morphologic and hemodynamic changes can be monitored over time (Fratz et al. 2013). Because of the variety in MR imaging sequences that can be used, imaging protocols may vary from simple and short to complex and extensive. We use sequences depending on the clinical question that has to be answered. A minimal standard follow-up protocol includes at least axial cine-series for assessing right and left

ventricular function and morphology (when the morphology is rather normal, the pulmonary morphology can often be evaluated on these images as well). Also, phase-contrast flow series of the pulmonary artery are made for assessing regurgitation and stenosis, series of the aortic valve for calculating shunt fraction by comparing flow with that of the pulmonary artery, and series of the tricuspid valve for assessing right ventricular diastolic function. Table 1 shows an overview of commonly used imaging sequences and their indications.

Table 1 Overview of MRI sequences and their purpose

Acquisition	Orientation	Purpose	Sequence
Localizer	–Axial –Sagittal –Coronal –Oblique	–Planning other sequences –Anatomical survey –Extracardial findings	
Black blood	–Axial –Sagittal –Coronal	–Cardiac anatomy	Double IR FSE
Single slice cine	–2-Chamber LV –2-Chamber RV –3-Chamber LV (LVOT) –4-Chamber (long axis) –RVOT	–Cardiac anatomy –Ventricular wall motion –Outflow obstruction	SSFP GE
Multi-slice cine	–Axial (preferred) –Ventricular short axis	–Cardiac anatomy –Ventricular wall motion –Outflow obstruction –Ventricular volume –Ventricular wall mass –Ventricular function	SSFP GE
Flow	Perpendicular to: –Proximal MPA –Proximal aorta –Mitral valve –Tricuspid valve	Quantifying: –Pulmonary flow –Systemic flow –Valve regurgitation –Peak flow velocity Assessment of ventricular diastolic dysfunction	PC GE
Flow	Perpendicular to: –Proximal LPA –Proximal RPA	Quantifying differential pulmonary artery flow	PC GE
Flow	4D dataset	Quantifying: –Pulmonary flow –Systemic flow –Valve regurgitation –Shunt fraction (direct shunt measurement) –Eccentric jets	PC GE echo planar
Late enhancement	–Ventricular short axis –2-Chamber LV –3-Chamber LV (LVOT) –4-Chamber	Myocardial scarring	Phase sensitive IR
Late enhancement	3D dataset	Myocardial scarring	Phase sensitive IR
MRA	Sagittal oblique	Vascular anatomy	3D spoiled GE

LV left ventricle, *RV* right ventricle, *LVOT* left ventricular outflow tract, *RVOT* right ventricular outflow tract, *MPA* main pulmonary artery, *LPA* left pulmonary artery, *RPA* right pulmonary artery, *ECG* electrocardiography-triggered, *IR* inversion recovery, *FSE* fast spin echo, *SSFP* steady-state free precession, *PC* phase-contrast, *GE* gradient echo

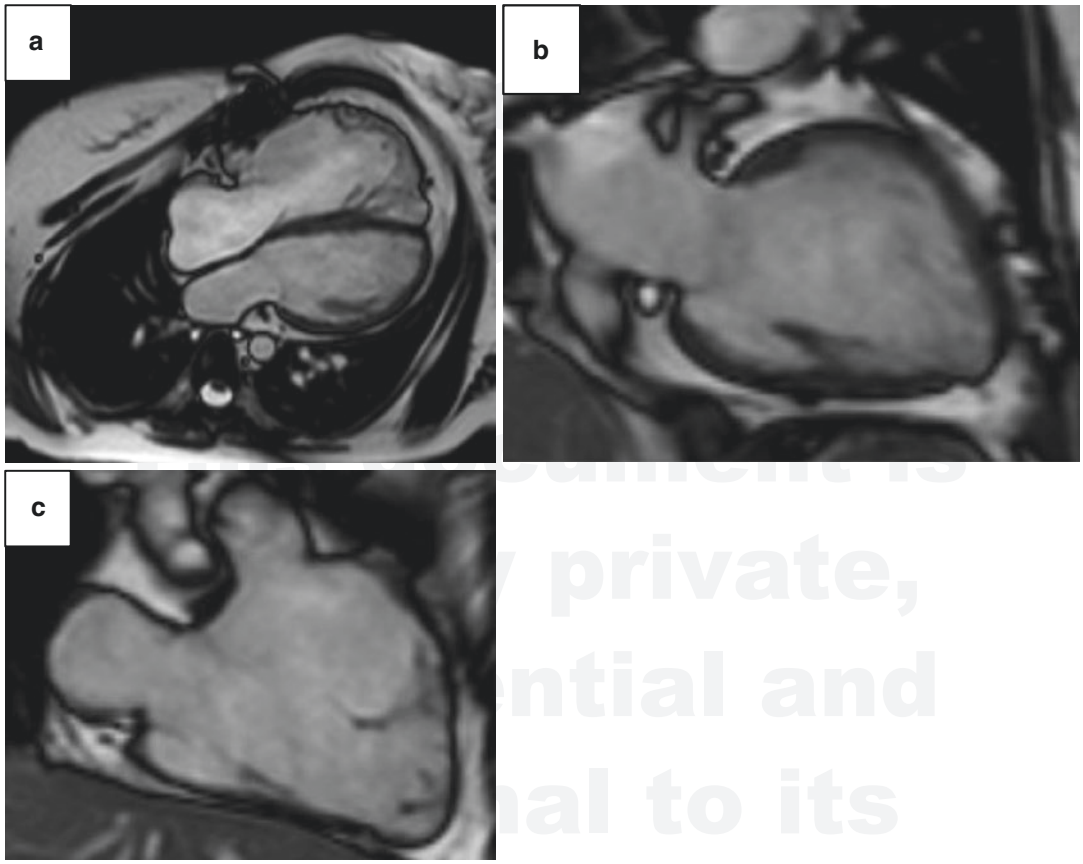

Fig. 10 Forty-nine-year-old female with corrected TOF. MRI bright blood (SSFP) images in axial (**a**), 2-chamber left (**b**), and 2-chamber right (**c**) view. Note the asymmetric chest wall, with ventral displacement at the level of the dilated right ventricle. SSFP images acquired throughout the cardiac cycle allow for visual assessment of ventricular size, function, and wall motion

In general, SSFP (steady-state free precession gradient-echo technique) imaging is typically used for imaging and measuring ventricular function and mass, as well as for visualizing valve leaflets and to assess the cardiac and surrounding anatomy. Images are acquired at standard cardiac planes (e.g., 2-chamber, 3-chamber, and 4-chamber views) throughout the cardiac cycle and allow for the visual assessment of ventricular function, wall motion, and valve function (Fig. 10). Continuous stacks of cine images are acquired in axial plane and include the entire ventricles to allow for reliable quantification of the ventricular end-diastolic and end-systolic volumes, as to calculate stroke volume and ejection fraction. Because the right ventricular morphology, global and regional function are best evaluated on axial ("transverse") series, and the left ventricle can be adequately evaluated regarding volumes and ejection fraction on these series as well, axial series are preferred over "left ventricular short-axis views" in TOF patients. Double inversion recovery (IR) fast spin-echo (FSE) sequences, also known as "black blood imaging" (Fig. 11), or ECG-triggered, respiratory-navigated SSFP "white blood" sequences can be used to produce high-resolution, high-contrast static images (Valente et al. 2014).

Furthermore, non-contrast and contrasted-enhanced MR angiography sequences allow for

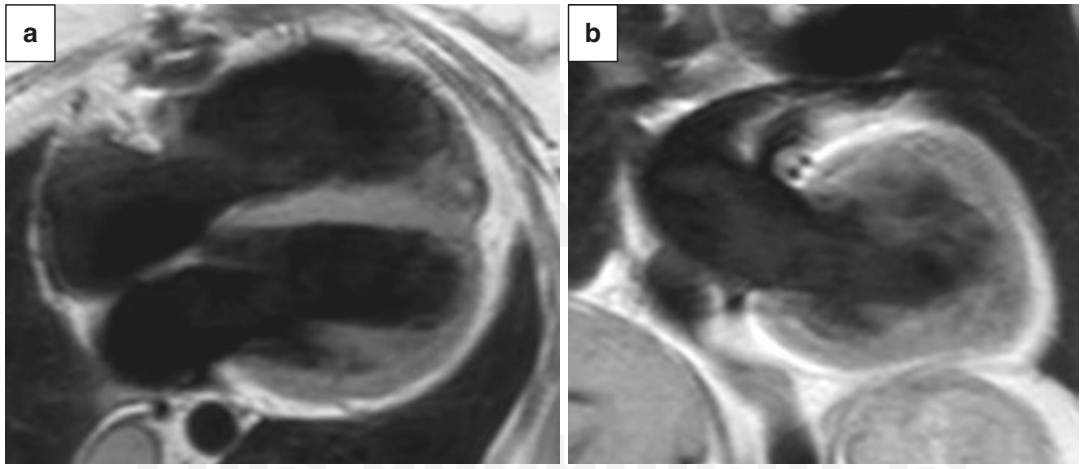

Fig. 11 Same patient as in Fig. 10. MRI black blood (double IR FSE) images in axial view (**a**) and coronal view (**b**). Black blood sequences produce high-resolution, high-contrast static images

the acquisition of 3D datasets for the assessment of systemic and pulmonary vessels and ECG-triggered phase-contrast sequences may be used to measure blood flow and quantify valve regurgitation fractions. Late enhancement sequences allows for the assessment of myocardial scaring and fibrosis after surgical correction.

3.4.1 Ventricular Volume and Function

Cardiac MRI is the reference standard for quantification of the ventricular volume and mass. To determine the volume of a ventricle, the blood pool area on all slices on which the ventricle is visible (n) is pooled and multiplied with the slice thickness according to the equation:

$$\text{Volume}\left(mL\right) = \sum_{i=1}^{n} \text{blood pool area}_i \left(mm^2\right) \times \text{slice thickness}\left(mm\right).$$

For calculating the blood pool volume, the area is drawn on each slice at the endocardium-blood boundary. Papillary muscles and trabeculations may be included or excluded from the blood pool volume; this should be done so consistently for end-systolic and end-diastolic phases to avoid over- or underestimation of volumes and function. Also, this should be done consistently during follow-up to allow for reliable comparison of volumes over time. Volumes are traced in end-diastolic and end-systolic phases (Fig. 12) and the difference between these two volumes represents the stroke volume:

Stroke volume (mL) = end diastolic volume (mL) – end systolic volume (mL).

From this, the ejection fraction and cardiac output can be calculated:

$$\text{Ejection fraction}\left(\%\right) = \frac{\text{stroke volume}\left(mL\right)}{\text{end diastolic volume}\left(mL\right)}$$

and

$$\text{Cardiac output}\left(\frac{mL}{min}\right) = \text{stroke volume}\left(mL\right) \times \text{heart rate}\left(bpm\right).$$

In patients with surgically corrected TOF, particular attention should be paid to selecting the correct end-diastolic and end-systolic phases for each ventricle individually, as these may differ due to conduction delay in the right ventricle (Geva 2011).

The ventricular mass can be calculated the same way by additionally tracing the epicardial border of the ventricle, thus creating an epicardial volume. The difference between the epicardial

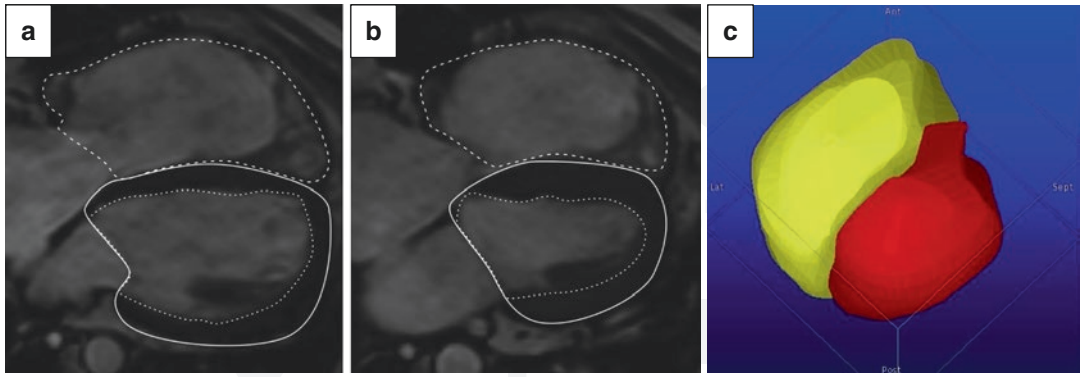

Fig. 12 Same patient as in Fig. 10. Volume tracing on MRI cine images. The blood pool area of the left ventricle (*fine dotted line*) and right ventricle (*dotted line*) are traced in end-diastolic (**a**) and end-systolic (**b**) phase. From this the ventricular volume and function can be calculated (volume rendering of both ventricles shown in **c**). End-diastolic volumes for left and right ventricles are 156 mL and 358 mL, respectively. End-systolic volumes for left and right ventricles are 74 mL and 264 mL, respectively. Stroke volume of the left ventricle is 82 mL, of the right ventricle is 94 mL. Ejection fractions: 52% and 26%, respectively. By tracing the epicardial contours the mass can be calculated, for the left ventricle (*continuous line*). This is 191 g. Similarly, this can be done for the right ventricle, but is less reliable

volume and blood pool volume results in the ventricular wall muscle volume that can be converted to mass by multiplying it with the specific gravity of myocardial muscle (1.05):

Ventricular wall mass (g) = (epicardial volume (mL) − blood pool volume (mL)) × 1.05.

Increased right ventricular mass in patients with surgically corrected TOF has been associated with increased risk of adverse outcomes. However, because of the complex right ventricular morphology, the right ventricular contours for mass calculation are rather difficult to analyze, with large variation in accuracy and reproducibility (Valente et al. 2014).

Table 2 shows normal values for end-systolic and end-diastolic volumes of the left and right ventricle, differentiated for gender and age decile, obtained from 120 healthy subjects (Maceira et al. 2006). In the follow-up of TOF patients it is important to determine the volume and function for both ventricles. The ejection fractions of the right and left ventricle are closely correlated and right ventricular dilatation and dysfunction may lead to left ventricular dysfunction (Geva et al. 2004). Systolic dysfunction of the left ventricle is present in 20% of patients with surgically corrected TOF, and is strongly associated with arrhythmia (Broberg et al. 2011; Khairy et al. 2010). In a multivariate analysis on patients with repaired TOF, a left ventricular ejection fraction below 55% showed to be an independent predictor for major adverse clinical outcome including death, sustained VT, and progression to NYHA class III or IV (Knauth et al. 2008).

Surgically corrected TOF patients may have impaired diastolic function of the right ventricle (Van den Berg et al. 2007). Diastolic ventricular filling happens by active relaxation of the myocardium at early diastole (the E-wave) and passive relaxation at late diastole (the A-wave, during atrial contraction). The two major determinants of ventricular filling are ventricular relaxation and chamber compliance, reflected by the inflow pattern of blood from the atrium. The inflow patterns of the right and left ventricles can be evaluated by means of the flow curves across the tricuspid valve and mitral valve, respectively. Measured variables include peak velocities of the E-wave and A-wave and the deceleration time of the E-wave. The E/A-ratio represents the difference between the peak velocities of the E-wave and A-wave. The E-wave is influenced by atrial pressure at atrioventricular valve opening and the rate of ventricular relaxation. The A-wave occurs at atrial contraction after ventricular relaxation, and depends on ventricular compliance.

Table 2 Normal absolute end-diastolic (EDV) and end-systolic (ESV) volumes in mL, papillary muscles excluded from volume

	Normal left ventricular volumes					
Males	20–29	30–39	40–49	50–59	60–69	70–79
EDV	126–208	121–204	117–200	113–196	109–191	105–187
ESV	35–80	33–78	31–76	29–74	27–72	25–70
EDV/BSA	68–103	66–101	64–99	62–97	60–95	58–93
ESV/BSA	19–41	18–39	17–38	15–37	14–36	13–35
Females	20–29	30–39	40–49	50–59	60–69	70–79
EDV	112–193	108–189	104–185	100–181	96–177	91–172
ESV	32–73	30–71	28–69	26–67	24–65	21–62
EDV/BSA	67–101	64–98	62–96	59–93	57–91	54–88
ESV/BSA	19–39	18–38	16–36	15–35	14–34	12–32
	Normal right ventricular volumes					
Males	20–29	30–39	40–49	50–59	60–69	70–79
EDV	127–227	121–221	116–216	111–210	105–205	100–200
ESV	38–98	34–94	29–89	25–85	20–80	16–76
EDV/BSA	68–114	65–111	62–108	59–105	56–101	52–98
ESV/BSA	21–50	18–47	16–45	13–42	11–40	8–37
Females	20–29	30–39	40–49	50–59	60–69	70–79
EDV	100–184	94–178	87–172	81–166	75–160	69–153
ESV	29–82	25–77	20–72	15–68	11–63	6–58
EDV/BSA	65–102	61–98	57–94	53–90	49–86	45–82
ESV/BSA	20–45	17–43	14–40	11–37	8–34	6–32

Data adapted from Maceira et al. 2006a and b. 95% confidence interval of normal ventricular volumes per age decile for adult males and females (10 subjects per subdivision, 120 subjects in total). Values indexed to body surface area (BSA) in mL/m^2 (mean BSA in males was 1.96, mean BSA in females was 1.71)

Normal diastolic function has an E/A-ratio > 1. Impaired relaxation is the earliest manifestation of diastolic dysfunction. Impaired relaxation leads to a lower early filling velocity (lower E-wave peak, with prolonged E-wave deceleration time). A compensatory increased flow at atrial contraction leads to an increased A-wave peak. The E/A-ratio may become reversed (<1) (Fig. 13). This flow pattern also occurs naturally with physical aging and is usually seen in patients over 70 years (Strait et al. 2012). With progressive decrease of ventricular compliance, diastolic dysfunction increases. High atrial pressure at atrioventricular valve opening leads to fast early filling of the ventricle (high E-wave peak). A more rapid increase in ventricular pressure shortens the E-wave deceleration time. The increased ventricular pressure also hampers forward flow during atrial contraction, leading to a lower A-wave peak. The flow pattern of decreased ventricular compliance (also referred to as restriction to ventricular filling) thus resembles the flow pattern of normal diastolic function with E/A-ratio > 1. This phenomenon is referred to as pseudo-normalization of the E/A-ratio. Determining the flow direction in the inferior vena cava or hepatic veins may aid in distinguishing normal right ventricular diastolic function from pseudo-normalization. Normal flow in the veins has a forward direction during systole and diastole and a retrograde direction during atrial contraction. With decreased compliance of the ventricle, forward flow decreases and retrograde flow during atrial contraction increases. The ratio between ventricular forward flow and retrograde venous flow is an indicator of ventricular compliance. With further progression of restrictive filling the E-wave increases and E-wave deceleration time decreases, leading to a steep, short E-wave. In severe diastolic dysfunction, the E/A-ratio

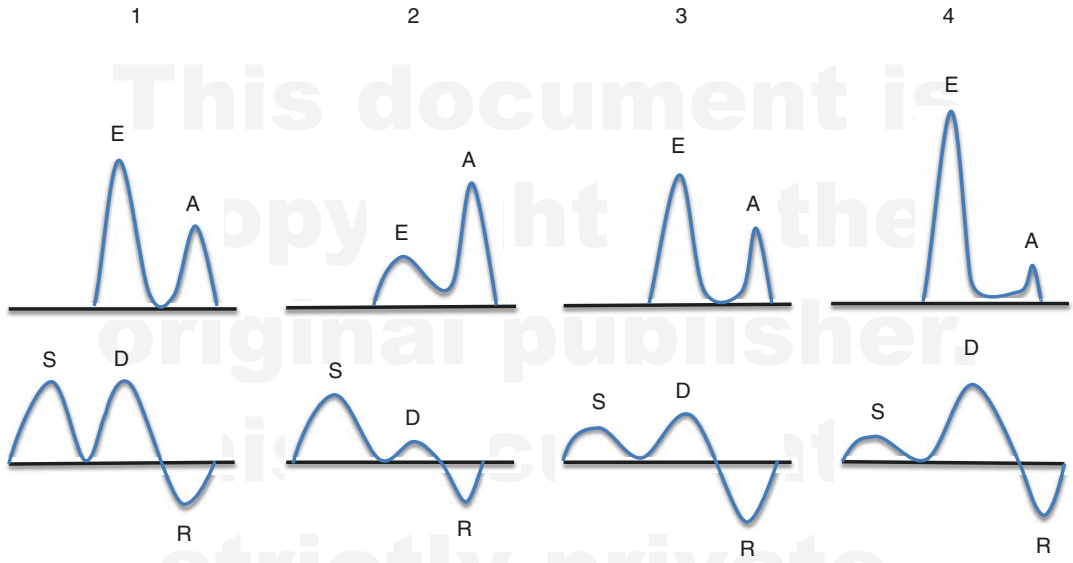

Fig. 13 Atrioventricular valve flow patterns (*upper row*) with early ventricular filling (E-wave) and ventricular filling during atrial contraction (A-wave) in normal diastolic function (*1*), impaired relaxation (*2*), reduced ventricular compliance or "pseudo-normalization" (*3*), and severe restriction to ventricular filling (*4*). In the lower row associated flow patterns in pre-atrial veins (*S* systolic flow, *D* diastolic flow, *R* retrograde flow during atrial contraction)

usually becomes >2 (Nishimura et al. 1997). Noteworthy, age-dependent variation, respiration, and inter-individual variation may hamper interpretation of inflow patterns. Furthermore, care should be taken to correct for pulmonary regurgitation, especially while interpreting the patterns in TOF patients.

The fundamental abnormality of impaired relaxation/restriction to right ventricle filling in TOF patients is ventricular hypertrophy due to an increased afterload of the right ventricle (Lam et al. 2007). The decreased compliance of the right ventricle leads to filling resistance. When this filling resistance exceeds the pulmonary vascular resistance, the right ventricle acts as conduit between the right atrium and pulmonary artery. As a result end-diastolic antegrade flow in the pulmonary artery may be observed. End-diastolic antegrade flow is present in a significant portion of TOF patients (Gatzoulis et al. 1995a; Van den Berg et al. 2007). Reports on the presence of restrictive physiology in adult TOF patients during long-term follow-up have been equivocal. Interestingly, some authors have found a protective effect on exercise performance (Gatzoulis et al. 1995b), while others found an association with severe pulmonary regurgitation and decreased exercise capacity (Van den Berg et al. 2007). These different results have been explained by different methods used to assess diastolic dysfunction. 3D velocity-encoded MR imaging may provide more accurate diastolic flow measurements than 2D techniques in assessing diastolic function (Van der Hulst et al. 2010). 3D velocity-encoded MR confirmed impaired right ventricular relaxation and restrictive right ventricular filling in TOF patients with end-diastolic antegrade flow in the pulmonary artery. This may help in assessing right ventricular diastolic dysfunction (Van der Hulst et al. 2010).

3.4.2 Right Ventricular Outflow Tract

Reconstruction of the right ventricular outflow tract is part of the corrective surgery procedure in TOF. Long-term pulmonary regurgitation affects the reconstructed outflow tract. Dilatation and wall motion abnormalities (akinesia and dyskinesia) are commonly observed in the right ventricular outflow tract. Wall

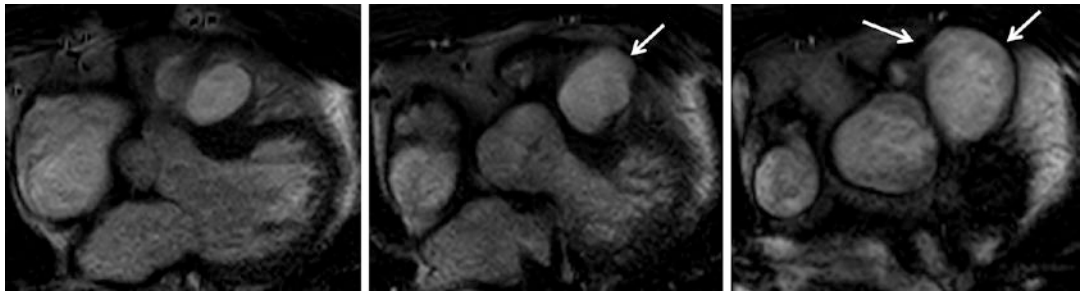

Fig. 14 Fifty-six-year-old male with corrected TOF. MRI bright blood (SSFP) images in three adjacent axial views of the RVOT, showing an aneurysm (*arrows*). SSFP cine images provide dynamic anatomical information about outflow tract dilatation or obstruction

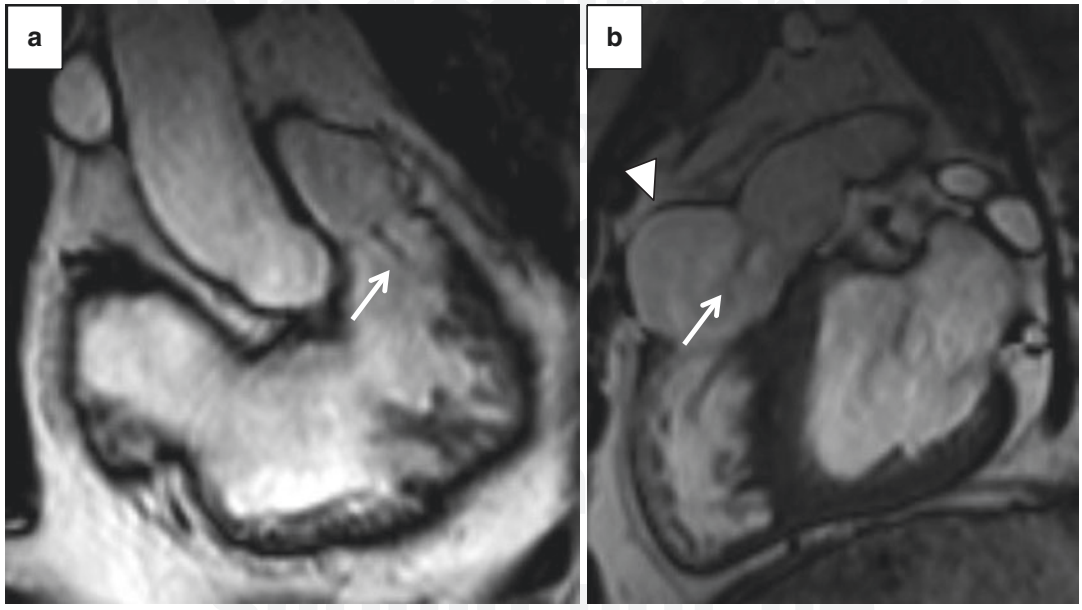

Fig. 15 Same patients as in Fig. 14. MRI bright blood (SSFP) images in 2-chamber view of the right ventricle (**a**) and RVOT view (**b**), demonstrating a flow-related jet caused by pulmonary regurgitation (*arrows*). Note the aneurysm of the RVOT in (**b**) (*arrowhead*)

motion abnormalities can be assessed using SSFP cine images. Evaluation can be done in the standard axial plane, as well as in outflow tract oriented 2-chamber and sagittal oblique views (Fig. 14). SSFP images provide dynamic anatomical information on outflow tract dilatation or obstruction, and flow-related signal loss or flow jets may be observed depending on the technique used (Fig. 15). Signal voids on SSFP images are related to acceleration rather than velocity, while SSFP images allow for visual assessment of turbulent flow, they may underestimate the degree of flow disturbance (Myerson 2012). In case of dilatation and aneurysm formation, SSFP images may depict thrombus at locations of slow flow. Furthermore, assessment of the right ventricular outflow tract morphology is necessary before considering percutaneous pulmonary valve replacement. A pyramidal shape of the right ventricular outflow tract, as can be seen in patients with previous transannular patch repair, is unsuited for percutaneous valve replacement (Saremi et al. 2013).

3.4.3 Pulmonary Valve and Pulmonary Arteries

Flow through the pulmonary arteries can be assessed using phase-contrast sequences and flow velocity measurements can aid in determining the severity of pulmonary branch stenosis. ECG-triggered phase-contrast sequences are used for flow measurements and quantification of pulmonary regurgitation (Fig. 16). The imaging plane is perpendicular to flow in the main pulmonary artery. Regurgitation percentage is calculated by dividing backward flow by forward flow and pulmonary valve regurgitation can be graded as mild (<20%), moderate (20–40%), or severe (>40%) (Mercer-Rosa et al. 2012).

Phase-contrast imaging can also be used to determine peak flow velocity that allows calculating the hemodynamic significance of a stenosis by applying the modified (simplified) Bernoulli equation (Wallerson et al. 1987): $\Delta P(\text{mmHg}) = 4 \times \upsilon^2 \left(\frac{\text{m}}{\text{sec}}\right)$, where the pressure

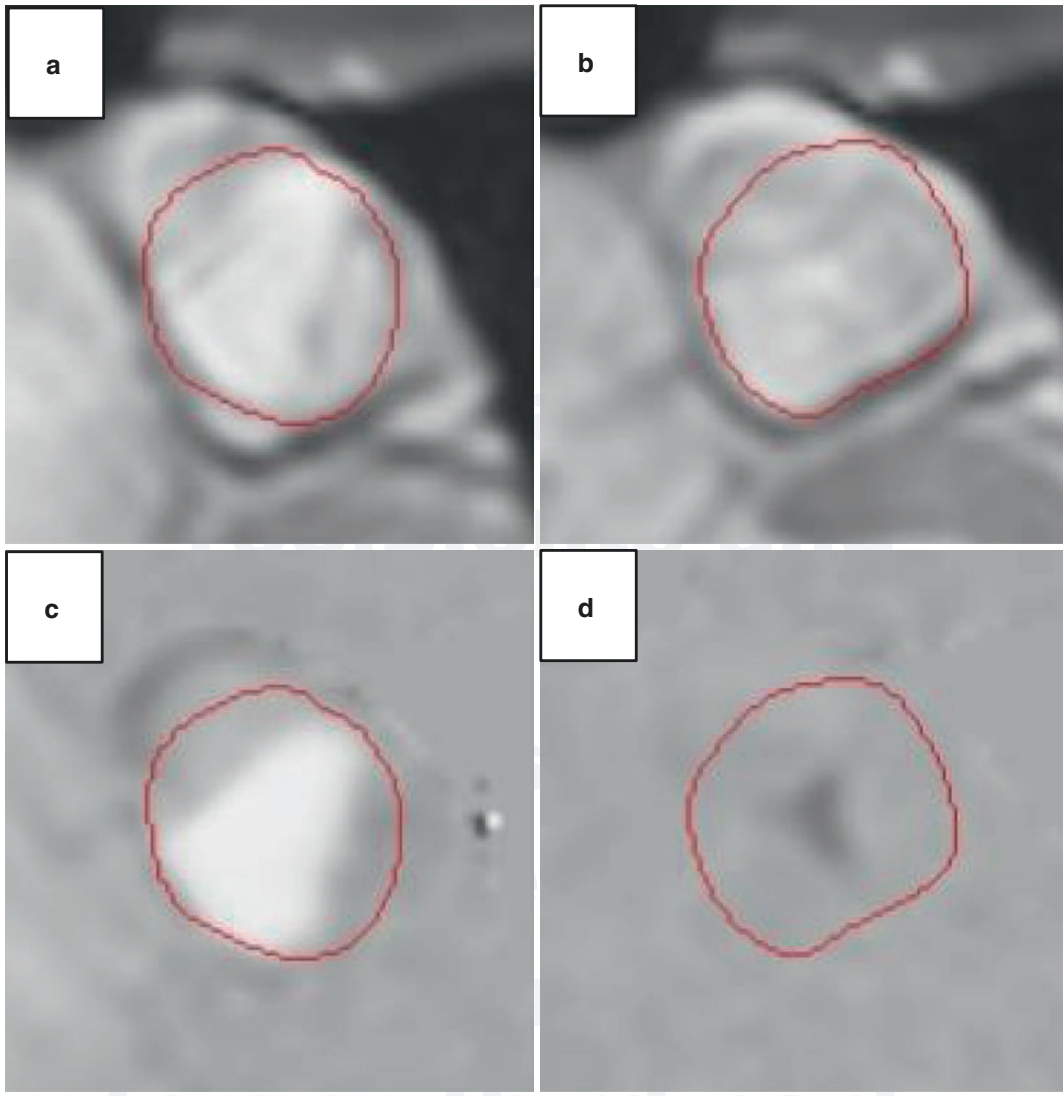

Fig. 16 Fifty-two-year-old male with corrected TOF. MRI anatomical modulus images (**a**, **b**) and phase-contrast (PC) images (**c**, **d**) showing pulmonary valve regurgitation. Systolic forward flow (*bright signal*) in the pulmonary artery at the level of the pulmonary valve (**a**, **c**). Backward flow (note that the signal is *black*, due to opposed flow direction) during diastole, indicating regurgitation (**b**, **d**). The flow over the valve can be quantified by drawing contours on the phase-contrast images (see graph): forward flow: 85 mL (above baseline), backward flow: 11 mL (below baseline). The net forward flow is 74 mL. Regurgitation fraction: 13% (backward flow divided by forward flow)

Fig. 16 (continued)

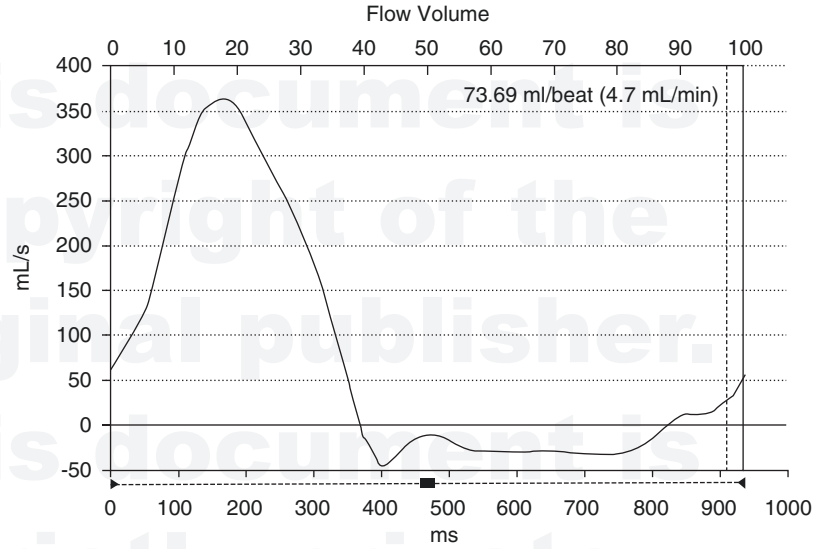

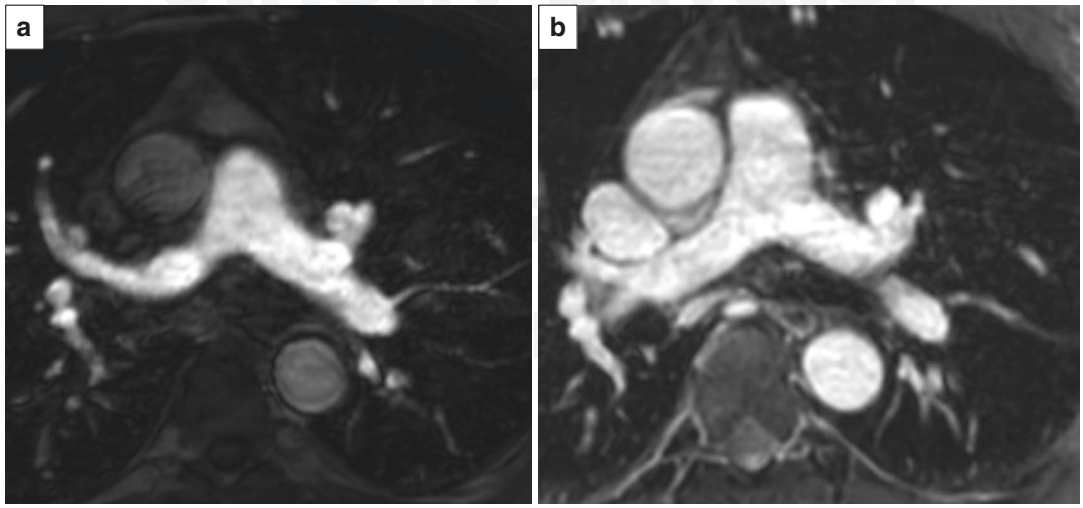

Fig. 17 Fifty-two-year-old male with corrected TOF. Contrast-enhanced MRA (**a**) of the pulmonary artery. MRA can be used to evaluate pulmonary artery (branch) stenosis. Alternative MRI sequences can produces comparable images without contrast (**b**, courtesy prof. H.J. Lamb)

(*P*) gradient equals four time the squared flow velocity distal from the stenosis (v^2). For example, the calculated pressure gradient over a stenosis with a measured peak flow velocity of 3.5 m/s is 49 mmHg. No absolute pressure gradient has been reported that indicates therapeutic intervention in TOF patients, however, a high systolic pressure in the right ventricle equal or larger than 70% of the systolic pressure in the systemic circulation could be considered an indication for pulmonary valve replacement (see also below).

Pulmonary artery or pulmonary artery branch stenosis may lead to pressure overload and right ventricular hypertrophy. Stenosis can be depicted anatomically by a variety of sequences, including static black blood (Double IR FSE) or white blood (SSFP) sequences or dynamic cine white blood techniques (SSFP). Contrast-enhanced MRA techniques can be used as well. MRA sequences provide a three-dimensional datasets which aids the visualization of the pulmonary arteries in relation to their anatomic surroundings and can be used for the evaluation of branch stenosis (Fig. 17). Excellent agreement between MRA and conventional angiography has been demonstrated (Greil et al. 2002). Regarding (pulmonary artery)

stent evaluation, FSE sequences have a high spatial resolution and are less susceptible to metal artifacts as compared to (contrast-enhanced) MRA, and may therefore provide additional information. The best sequence for determining in-stent stenosis with MRI is subject of ongoing research and improves over time with new developments in MRI techniques. By comparing flow measurements between the right and left pulmonary artery, flow differences between the lungs can be calculated (Weber et al. 2006).

3.4.4 Myocardial Scarring/Fibrosis

Late enhancement (or late gadolinium enhancement, LGE, also known as "delayed enhancement") refers to the presence of bright signal in the myocardium 15–20 min after administration of gadolinium contrast. After injection, gadolinium contrast reaches the myocardial interstitial space via the coronary circulation and washes out from the normal interstitium within approximately 10 min. Gadolinium contrast is retained in areas with increased extracellular space, such as in acute or chronic myocardial infarction. Late enhancement may also be seen in myocarditis, various cardiomyopathies, and myocardial storage diseases (Vogel-Claussen et al. 2006).

In TOF patients, late enhancement is common at locations of surgical corrections, such as the right ventricular outflow tract and in and around patched septal defects, due to retention of gadolinium contrast in scarred or fibrotic tissue. In patients who underwent surgery with the use of a transapical vent in the left ventricle, focal transmural late enhancement may be observed at the insertion point at the left ventricular apex (Babu-Narayan et al. 2006).

In TOF, late enhancement may also be typically observed in the right ventricular anterior wall and at the junction points of the right ventricle and the ventricular septum. The reason for late enhancement at these sites is unclear, but most likely reflects previous myocardial damage that occurred early in life, perioperative, or progressively due to myocardial strain. One hypothesis for enhancement at these particular locations is progressive right ventricular fibrosis from stretching, dilatation, and hypertrophy, due to pulmonary regurgitation or stenosis (Babu-Narayan et al. 2006). Late enhancement at these locations has been associated with ventricular dysfunction, arrhythmias, and exercise intolerance (Oosterhof et al. 2005; Babu-Narayan et al. 2006; Wald et al. 2009).

Identification of areas of myocardium scarring may guide treatment of patients with arrhythmias by radio frequency or cyro-catheter ablation therapy. Catheter ablation is generally performed under fluoroscopy guidance, where using the late enhancement MRI containing scar focus information in the electro-anatomical mapping system can facilitate the mapping procedure and aid in planning ablation therapy (Kolandaivelu et al. 2009).

3.4.5 Aortic Root

Aortic root dilatation is a known complication in TOF that may lead to aortic valve regurgitation that needs surgery. The reported incidence ranges from 15 to 88% (Grotenhuis et al. 2009). Dilatation may result from increased aortic flow from right-to-left shunting prior to corrective surgery (Niwa et al. 2002). However, dilatation has also been shown to progress after surgery. It has been hypothesized that hemodynamic stress leads to damage of the aortic wall media (Dobbs et al. 1997). MRI studies have shown that aortic dilatation could attribute to wall pathology indeed, as is reflected by abnormal aortic wall distensibility (Grotenhuis et al. 2009). Furthermore, reduced aortic elasticity may have a negative effect on aortic valve function (Grotenhuis et al. 2009).

Aortic root dilatation can be assessed with MRI using cine SSFP sequences parallel and perpendicular to the aortic root, as well as with ECG-triggered 3D SSFP sequences (Fig. 18). Similar to CT, measurements of the aortic diameter should be performed in double oblique fashion (perpendicular to the axis of blood flow) and include the vessel wall for reproducibility and comparison reasons.

Contrast-enhanced MRA may also be used for assessing aortic root dilatation, but it should be noted that images with non-ECG-triggered sequences can be blurred by motion artifacts (Kaiser et al. 2008). Aortic valve regurgitation can be quantified with phase-contrast imaging perpendicular to the aortic root.

3.4.6 Shunts

Shunts in TOF, such as a residual VSD or ASD after patch closure, are usually recognized with echocardiography, but can also be visualized with MRI using SSFP or TSE sequences

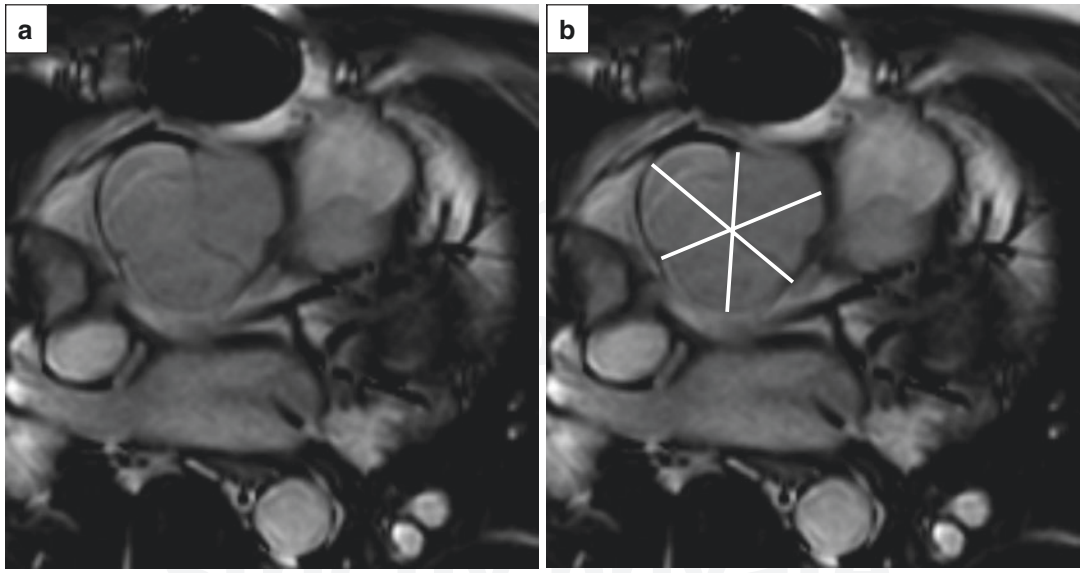

Fig. 18 Forty-four-year-old male with corrected TOF. MRI bright blood (SSFP) images of the aortic root, demonstrating aortic root dilatation (**a**). The mean cusp-commissure diameter can be measured at this level (**b**, *lines*). The mean diameter was 46 mm

perpendicular and in plane parallel to the atrioventricular septum. Flow over the septum defect can be quantified with phase-contrast imaging, which should be planned perpendicular to the direction of the jet. In case of an eccentric jet, the perpendicular plane may be difficult to establish at the time of acquisition. Non-perpendicular acquired phase-contrast images may underestimate the magnitude of the shunt flow. Four-dimensional, three-directional flow sequences may be used for optimal shunt calculation (Roes et al. 2009). Alternatively, to quantify a left-to-right shunt, the shunt ratio can be calculated by the formula Qp:Qs, where Qp represents the flow volume in the main pulmonary artery and Qs the flow volume in the ascending aorta (s, systemic). A shunt ratio > 1.5 is generally used as an indication for surgical closure (Baumgartner et al. 2010).

3.4.7 Timing Pulmonary Valve Replacement

The negative effect of pulmonary valve regurgitation and the resulting right ventricular volume overload is well known and has been extensively described in literature. Largely dilated right ventricles (e.g., EDV 172 mL/m^2 in female and 185 mL/m^2 in male) are associated with adverse outcomes (Knauth et al. 2008). Adult patients with too largely dilated right ventricles have also been shown to no longer benefit from pulmonary valve replacement (Thierrien et al. 2000). Preoperative thresholds for diastolic and systolic volumes have therefore been suggested; normalization of the right ventricular volume can be achieved when the EDV is <160 mL/m^2 before pulmonary valve replacement (Fig. 19) (Oosterhof et al. 2007). Nevertheless, consensus on optimal timing of pulmonary valve replacement is still lacking and may be especially difficult for asymptomatic patients (Apitz et al. 2009, Geva 2013). For timing surgery, the risk of the procedure has to outweigh the risk for further decline. According to the ESC guidelines, pulmonary valve replacement should be performed in symptomatic patients with severe pulmonary regurgitation and/or stenosis. Pulmonary valve replacement should also be considered in asymptomatic patients with severe pulmonary regurgitation and/or stenosis and objective decrease in exercise capacity, progressive right ventricular dilatation or systolic dysfunction, progressive tricuspid regurgitation, right ventricular outflow tract obstruction with right ventricular systolic pressure > 80 mmHg, or sustained atrial or ventricular arrhythmias (Baumgartner et al. 2010). Based on interpretation of available literature, Geva individually proposed similar

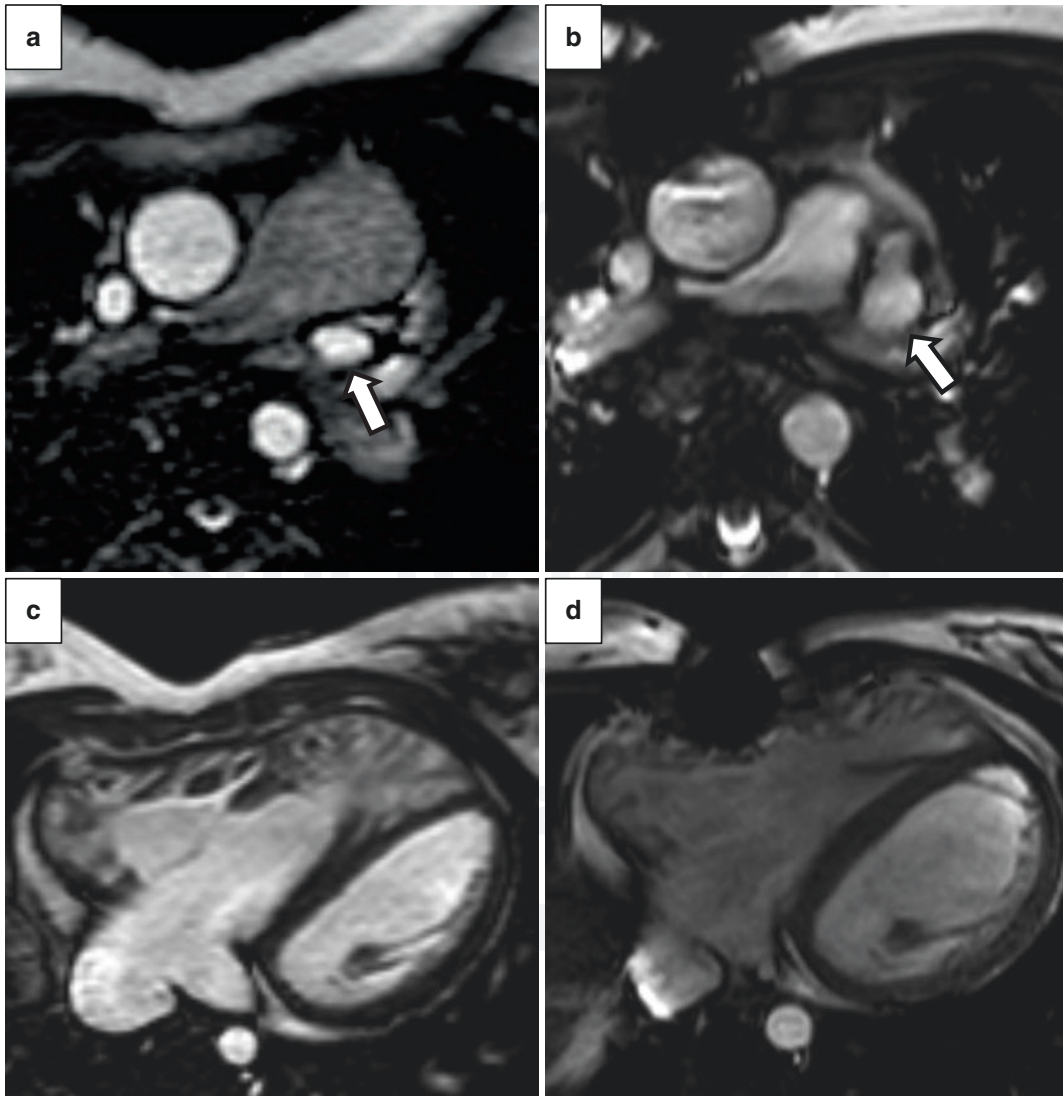

Fig. 19 Forty-four-year-old female with corrected TOF. MRI bright blood (SSFP) images of the pulmonary artery and right ventricle before (**a**, **c**) and after pulmonary valve replacement (**b**, **d**). Dilated pulmonary artery (**a**) and right ventricular dilatation and hypertrophy (**c**) before pulmonary valve replacement. After surgery pulmonary artery size has been normalized (**b**) and the right ventricular size decreased (**d**). Note the coexisting persist left superior vena cava (*arrows*) displaced backwards by the dilated pulmonary artery in (**a**)

indications for pulmonary valve replacement in repaired TOF patients, as well as some additional indications (Geva 2013). Table 3 summarizes the indications proposed in both publications.

Currently, the role of N-terminal B-type natriuretic peptide (NT-proBNP) is subject of investigation in the follow-up of TOF patients. NT-proBNP is a biomarker that reflects general cardiac function. In patients with chronic heart failure, NT-proBNP guided therapy has shown to reduce all-cause mortality (Troughton et al. 2014). Interestingly, in TOF patients increased NT-proBNP has been shown to correlate with deteriorated left ventricular MRI parameters (ejection fraction, mass, end-systolic and end-diastolic volume index), but not with any volumetric or functional parameters of the right ventricle. Moreover, NT-proBNP was shown superior to MRI regarding risk assessment. This suggests that while right ventricular parameters

Table 3 Proposed indications for pulmonary valve replacement

Indication for pulmonary valve replacement	
ESC recommended indications:	
Symptomatic patients	Additional 1 or more criteria for asymptomatic patients
Severe pulmonary regurgitation	Decrease in objective exercise capacity
Severe pulmonary stenosis (right ventricular systolic pressure > 60 mmHg)	Progressive right ventricular dilatation
	Progressive right ventricular systolic dysfunction
	Progressive tricuspid valve regurgitation (at least moderate)
	RVOT obstruction with right ventricular systolic pressure > 80 mmHg
	Sustained arrhythmias
Proposed indications by Geva based on available literature:	
Symptomatic patients with one or more of the following criteria or asymptomatic patients with two or more of the following criteria:	
Ventricular dilatation	Hemodynamic abnormalities
Right ventricular EDV index >150 mL/m^2	RVOT obstruction with right ventricular systolic pressure ≥ 0.7 systemic systolic pressure
Right ventricular ESV index >80 mL/m^2	Severe branch pulmonary artery stenosis (<30% flow to affected lung) not amenable to transcatheter therapy
Ventricular function	Pulmonary valve regurgitation greater than or equal to moderate tricuspid regurgitation
Right ventricular ejection fraction <47%	Left-to-right shunt from residual septal defects with pulmonary-to-systemic flow ratio ≥ 1.5
Left ventricular ejection fraction <55%	Severe aortic regurgitation
Conduction abnormalities	Morphologic abnormalities
QRS duration >160 ms	Large RVOT aneurysm
Sustained tachyarrhythmia related to right-sided heart volume load	

Adapted from Baumgartner et al. 2010 and Geva 2013.
RVOT right ventricular outflow tract

reflect severity of pulmonary regurgitation, left ventricular parameters are important for long-term clinical outcome (Westhoff-Bleck et al. 2016). Even in mildly symptomatic patients with pulmonary regurgitation after TOF repair, NT-proBNP was shown a strong predictor of adverse outcome (supraventricular tachycardia or heart failure).

Thus, while MRI plays a crucial role in the follow-up of morphological and functional changes that direct therapy, biomarkers such as NT-proBNP may be of additional prognostic value. Further research should include biomarkers to determine their value for timing pulmonary valve replacement (Westhoff-Bleck et al. 2016).

3.4.8 MRI Limitations

Cardiac MRI quality can be severely hampered by susceptibility artifacts caused by implants or other ferromagnetic objects (e.g., containing iron, nickel, or cobalt). These materials have positive magnetic susceptibility that affects the homogeneity of the magnetic field and results in signal loss and spatial distortion, observed as dark spots or areas that can hamper diagnosis. Furthermore, presence of a strong magnetic field and/or field changes during acquisition impose an absolute contraindication for patients with certain implanted electronic devices (e.g., neurostimulating devices). Until recently, having a pacemaker was considered an absolute contraindication for cardiac MRI. Nowadays many new implantable devices contain little or no ferromagnetic material and an increasing number of MRI-safe devices become available (Shinbane et al. 2011; Hwang et al. 2016). Patients with implanted pacemakers or defibrillators may be scanned, provided that (1) no alternative imaging modality for diagnosis (e.g., CT or echocardiography) is available, (2) the MRI examination is strongly indicated, (3) planning and performance of the MRI investigation follows strict guidelines and communication with involved clinicians/technicians, and (4) that the patient is not pacemaker-rhythm dependent (Horwood et al. 2016). In our department MRI procedures in these patients are performed under direct supervision of the radiologist at the MRI scanner and with clinical guidance by the cardiologist and/or pacemaker

technician. Relative contraindications exist for patients with residual epicardial pacemaker leads due to the possible risk of heat or electric current generation in the lead wires.

The MRI bore is generally small; the patient is positioned in the tight tunnel, while the examination time is usually long (between 30 and 60 min). This can be a contraindication for patients with severe claustrophobia. In milder cases sedation may help in performing the MRI examination.

Regarding risk, nephrogenic systemic fibrosis (NSF) is a rare but severe complication of gadolinium-bases contrast agents. NSF is characterized by skin thickening and tethering that causes flexion contractures of joints (Bernstein 2012). Patients with end-stage kidney disease (glomerular filtration rate (GFR) < 15 mL/min or on hemodialysis) are predominantly affected, but NSF has been reported in patients with less severe chronic kidney disease (Bernstein 2012). After recognition of the relation between gadolinium-based contrast agent administration and NSF, the U.S. Food and Drug Administration has recommended against using gadolinium-based contrast agents in patients with GFR <30 mL/min. Changes in guidelines and regulations have led to NSF occurrence decline to near zero since 2009 (Forghani 2016).

3.5 Nuclear Imaging

Historically, nuclear imaging has been used to evaluate cardiac function, myocardial perfusion, and to quantify blood flow in cardiac patients. Currently, cardiac MRI has replaced nuclear imaging as the first imaging modality of choice for many indications. MRI provides superior anatomic detail without radiation exposure (Valente et al. 2014). Nuclear imaging in TOF is reserved for quantification of (asymmetrical) lung perfusion in patients with contraindications for cardiac MRI. Asymmetrical lung perfusion may be observed in TOF patients with pulmonary artery stenosis that can be predictive for prognosis. The gold standard for quantifying pulmonary perfusion is quantitative perfusion scintigraphy with intravenous injection of radioactive Technetium-99m (99Tc) macroaggregated albumin (MAA). Count images of both lungs are acquired using a gamma camera (Fathala 2010). In TOF patients with normal pulmonary arteries, lung perfusion is comparable to the normal population, with slightly larger perfusion to the right lung than to the left lung reflecting the differences in lung volumes (Fathala 2010). In patients with pulmonary artery stenosis, scintigraphy may demonstrate segmental or unilateral hypoperfusion (Fig. 20).

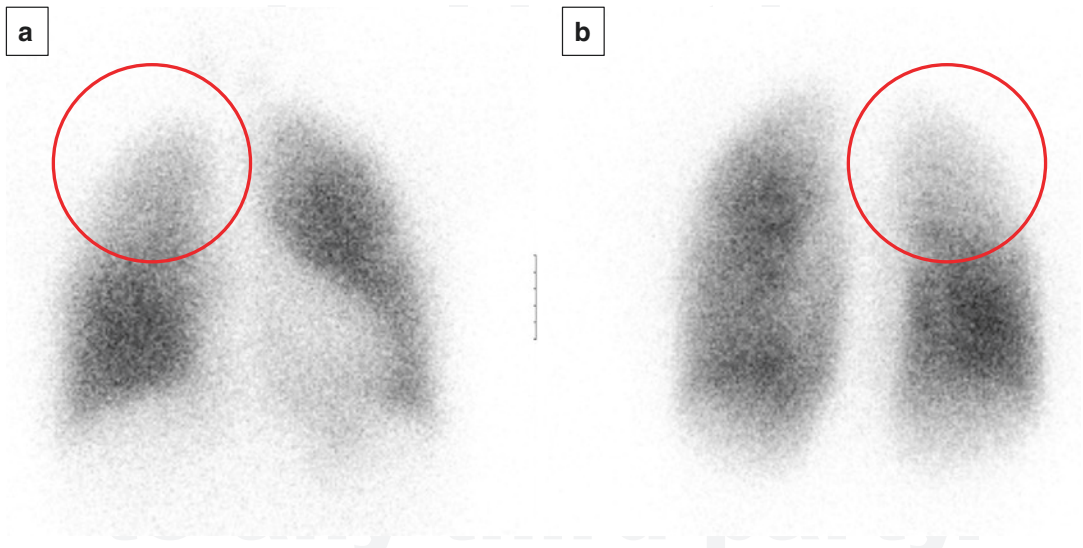

Fig. 20 Same patient as in Fig. 8. 99Tc-MAA perfusion scintigraphy in anterior (**a**) and posterior (**b**) view. Besides the stenosis of the right pulmonary artery, treated with a stent, right pulmonary branch stenosis was also suspected. Anterior and posterior views confirm a segmental hypoperfusion of the right upper lobe (*encircled*). Note that due to the shape and location of the heart less perfusion is seen in the left lower field in anterior view, but not in posterior view

Perfusion scintigraphy may guide decision-making for treating pulmonary artery or branch stenosis and can be used to evaluate the treatment effect.

Conclusion

Imaging plays an important role in the follow-up of patients with TOF and mainly focuses on the assessment of late complications after surgical corrections, in particular pulmonary valve regurgitation and right ventricular dilatation. Several imaging modalities are available for follow-up, including echocardiography, cardiac MRI, and cardiac CT.

Cardiac MRI is the imaging modality of first choice for the assessment of repaired TOF, because it allows for complete assessment of the cardiovascular morphology and physiology. Cardiac MRI provides reproducible and accurate measurements of the right ventricular volume and function, pulmonary flow volumes, regurgitation and stenosis, and has the ability to detect myocardial scarring. MRI is attractive as longitudinal follow-up imaging modality because of lack of harmful ionizing radiation.

Cardiac CT is a good alternative imaging modality for follow-up of patients with contraindication for cardiac MRI. CT can be safely performed in patients with implanted cardiac devices (e.g., pacemaker). CT provides excellent spatial resolution that allows for detailed visualization of complex cardiovascular anatomy and may be used as a complementary imaging modality in cases where MRI is inconclusive (e.g., evaluation of stent related complications).

Over the years, surgical correction of TOF has changed from complete relief of outflow obstruction at the expense of pulmonary valve regurgitation, towards accepting a residual obstruction but preserving pulmonary valve function, in order to prevent the late complications of right ventricular dilatation. A largely dilated right ventricle, but also left ventricular dysfunction determine outcome in TOF patients. Optimal timing of pulmonary valve replacement is difficult where the risk of surgery is weighted against the expected health benefits. MRI in particular plays a crucial role in detecting the morphological and functional changes that guide therapy.

References

Andreucci M et al (2014) Side effects of radiographic contrast media: pathogenesis, risk factors, and prevention. Biomed Res Int 2014:741018

Apitz C et al (2009) Tetralogy of Fallot. Lancet 374:1462–1471

Van Arsdell GS et al (2000) What is the optimal age for repair of tetralogy of Fallot? Circulation 102(Suppl 3):III123–III129

Van Arsdell G et al (2005) An apology for primary repair of tetralogy of Fallot. Semin Thorac Cardiovasc Surg Pediatr Card Surg Annu:128–131

Babu-Narayan SV et al (2006) Ventricular fibrosis suggested by cardiovascular magnetic resonance in adults with repaired tetralogy of Fallot and its relationship to adverse markers of clinical outcome. Circulation 113(3):405–413

Baumgartner B et al (2010) ESC guidelines for the management of grown-up congenital heart disease (new version 2010). Eur Heart J 31:2915–2957

Van den Berg J et al (2007) Diastolic function in repaired tetralogy of Fallot at rest and during stress: assessment with MR imaging. Radiology 243(1):212–219

Bernstein EJ et al (2012) Nephrogenic systemic fibrosis: a systemic fibrosing disease resulting from gadolinium exposure. Best Pract Res Clin Rheumatol 26(4):489–503

Bertranou EG et al (1978) Life expectancy without surgery in tetralogy of Fallot. Am J Cardiol 42:458–466

Berul CI et al (1997) Electrocardiographic markers of late sudden death risk in postoperative tetralogy of Fallot children. J Cardiovasc Electrophysiol 8:1349–1356

Boshoff D et al (2006) A review of the options for treatment of major aortopulmonary collateral arteries in the setting of tetralogy of Fallot with pulmonary atresia. Cardiol Young 16(3):212–220

Boxt LM (1999) Radiology of the right ventricle. Radiol Clin N Am 37(2):379–400

Brenner DJ et al (2003) Cancer risks attributable to low doses of ionizing radiation: assessing what we really know. Proc Natl Acad Sci U S A 100(24):13761–13766

Broberg CS et al (2011) Prevalence of left ventricular systolic dysfunction in adults with repaired tetralogy of Fallot. Am J Cardiol 107:1215–1220

Carminati M et al (2015) Echocardiographic assessment after surgical repair of tetralogy of Fallot. Front Pediatr 3:3

Carvalho JS et al (1992) Exercise capacity after complete repair of tetralogy of Fallot: deleterious effects of residual pulmonary regurgitation. Br Heart J 67:470–473

Chaturvedi RR et al (1997) Increased airway pressure and simulated branch pulmonary artery stenosis increase pulmonary regurgitation after repair of tetralogy of Fallot. Circulation 95:643–649

Chowdhury UK et al (2006) Histopathology of the right ventricular outflow tract and its relationship to clinical outcomes and arrhythmias in patients with tetralogy of Fallot. J Thorac Cardiovasc Surg 132:270–277

Coutu M et al (2004) Late myocardial revascularization in patients with tetralogy of Fallot. Ann Thorac Surg 77:1454–1455

Cullen S et al (1995) Characterization of right ventricular diastolic performance after complete repair of tetralogy of Fallot. Restrictive physiology predicts slow postoperative recovery. Circulation 91:1782–1789

Dobbs GA et al (1997) Aortic valve replacement after repair of pulmonary atresia and ventricular septal defect or tetralogy of Fallot. J Thorac Cardiovasc Surg 113(4):736–741

Fathala A (2010) Quantitative lung perfusion scintigraphy in patients with congenital heart disease. Heart Views 11(3):109–114

Forghani R (2016) Adverse effects of gadolinium-based contrast agents: changes in practice patterns. Top Magn Reson Imaging 25(4):163–169

Fratz S et al (2013) Guidelines and protocols for cardiovascular magnetic resonance in children and adults with congenital heart disease: SCMR expert consensus group on congenital heart disease. J Cardiovasc Magn Reson 15:51

Gatzoulis MA et al (1995a) Right ventricular diastolic function 15 to 35 years after repair of tetralogy of Fallot. Restrictive physiology predicts superior exercise performance. Circulation 91:1775–1781

Gatzoulis MA et al (1995b) Mechanoelectrical interaction in tetralogy of Fallot. QRS prolongation relates to right ventricular size and predicts malignant ventricular arrhythmias and sudden death. Circulation 92(2):231–237

Geva T et al (2004) Factors associated with impaired clinical status in long-term survivors of tetralogy of Fallot repair evaluated by magnetic resonance imaging. J Am Coll Cardiol 43:1068–1074

Geva T (2011) Repaired tetralogy of Fallot: the roles of cardiovascular magnetic resonance in evaluating pathophysiology and for pulmonary valve replacement decision support. J Cardiovasc Magn Reson 13:9

Geva T (2013) Indications for pulmonary valve replacement in repaired tetralogy of Fallot: the quest continues. Circulation 128(17):1855–1857

Greil GF et al (2002) Coronary magnetic resonance angiography in adolescents and young adults with kawasaki disease. Circulation 105(8):908–911

Grotenhuis et al. (2009) Aortic elasticity and size are associated with aortic regurgitation and left ventricular dysfunction in tetralogy of Fallot after pulmonary valve replacement. Heart 95:1931–1936

Haider EA (2008) The boot-shaped heart sign. Radiology 246(1):328–329

Al Habib HF et al (2010) Contemporary patterns of management of tetralogy of Fallot: data from the Society of Thoracic Surgeons database. Ann Thorac Surg 90:813–819

Hamdan A et al (2011) A prospective study for comparison of MR and CT imaging for detection of coronary artery stenosis. JACC Cardiovasc Imaging 4(1):50–61

Hiratzka LF et al (2010) ACCF/AHA/AATS/ACR/ASA/SCA/SCAI/SIR/STS/SVM guidelines for the diagnosis and management of patients with thoracic aortic disease: a report of the American College of Cardiology Foundation/American Heart Association Task Force on Practice Guidelines, American Association for Thoracic Surgery, American College of Radiology, American Stroke Association, Society of Cardiovascular Anesthesiologists, Society for Cardiovascular Angiography and Interventions, Society of Interventional Radiology, Society of Thoracic Surgeons, and Society for Vascular Medicine. Circulation 121(13):e266–e369

Horwood L et al (2016) Magnetic resonance imaging in patients with cardiac implanted electronic devices: focus on contraindications to magnetic resonance imaging protocols. Europace. pii: euw122

Van der Hulst AE et al (2010) Tetralogy of Fallot: 3D velocity-encoded MR imaging for evaluation of right ventricular valve flow and diastolic function in patients after correction. Radiology 256(3):724–734

Van der Hulst AE et al (2011) Real-time three-dimensional echocardiography: segmental analysis of the right ventricle in patients with repaired tetralogy of fallot. J Am Soc Echocardiogr 24(11):1183–1190

Hwang YM et al (2016) Cardiac implantable electronic device safety during magnetic resonance imaging. Korean Circ J 46(6):804–810

Iriart X et al (2009) Right ventricle three-dimensional echography in corrected tetralogy of Fallot: accuracy and variability. Eur J Echocardiogr 10(6):784–792

Jahangiri M et al (1999) Does the modified Blalock-Taussig shunt cause growth of the contralateral pulmonary artery? Ann Thorac Surg 67(5):1397–1399

Joemai RM et al (2008) Clinical evaluation of 64-slice CT assessment of global left ventricular function using automated cardiac phase selection. Circ J 72(4):641–646

Johnson C (1965) Fallot's tetralogy: a review of the radiological appearances in thirty-three cases. Clin Radiol 16:199–210

Kaiser T et al (2008) Normal values for aortic diameters in children and adolescents—assessment in vivo by contrast-enhanced CMR-angiography. J Cardiovasc Magn Reson 10:56

Karl TR et al (1992) Tetralogy of Fallot: favorable outcome of nonneonatal transatrial, transpulmonary repair. Ann Thorac Surg 54:903–907

Khairy P et al (2010) Arrhythmia burden in adults with surgically repaired tetralogy of Fallot: a multi- institutional study. Circulation 122:868–875

Khoo NS et al (2009) Assessments of right ventricular volume and function using three-dimensional echocardiography in older children and adults with congenital heart disease: comparison with cardiac

magnetic resonance imaging. J Am Soc Echocardiogr 22:1279–1288
Kilner PJ et al (2010) Recommendations for cardiovascular magnetic resonance in adults with congenital heart disease from the perspective workings groups of the European Society of Cardiology. Eur Heart J 31:794–805
Knauth AL et al (2008) Ventricular size and function assessed by cardiac MRI predict major adverse clinical outcomes late after tetralogy of Fallot repair. Heart 94(2):211–216
Koestenberger M et al (2011) Tricuspid annular plane systolic excursion and right ventricular ejection fraction in pediatric and adolescent patients with tetralogy of Fallot, patients with atrial septal defect, and age-matched normal subjects. Clin Res Cardiol 100(1):67–75
Kolandaivelu A et al (2009) Cardiovascular magnetic resonance guided electrophysiology studies. J Cardiovasc Magn Reson 11(1):21
Lam YY et al (2007) Restrictive right ventricular physiology: its presence and symptomatic contribution in patients with pulmonary valvular stenosis. J Am Coll Cardiol 50(15):1491–1497
Lanjewar C et al (2012) Aneurysmally dilated major aorto-pulmonary collateral in tetralogy of Fallot. Indian Heart J 64(2):196–197
Lembcke A et al (2005) Multislice computed tomography for preoperative evaluation of right ventricular volumes and function: comparison with magnetic resonance imaging. Ann Thorac Surg 79(4):1344–1351
Maceira AM et al (2006a) Reference right ventricular systolic and diastolic function normalized to age, gender and body surface area from steady-state free precession cardiovascular magnetic resonance. Eur Heart J 27(23):2879–2888
Maceira AM et al (2006b) Normalized left ventricular systolic and diastolic function by steady state free precession cardiovascular magnetic resonance. J Cardiovasc Magn Reson 8(3):417–426
McElhinney DB (2011) Stent fracture, valve dysfunction, and right ventricular outflow tract reintervention after transcatheter pulmonary valve implantation: patient-related and procedural risk factors in the US Melody Valve Trial. Circ Cardiovasc Interv 4(6):602–614
Mercer-Rosa L et al (2012) Quantifying pulmonary regurgitation and right ventricular function in surgically repaired tetralogy of Fallot: a comparative analysis of echocardiography and magnetic resonance imaging. Circ Cardiovasc Imaging 5(5):637–643
Miyazaki O et al (2001) Sudden death due to rupture of major aortopulmonary collateral arteries in a patient with tetralogy of Fallot and pulmonary atresia. Emerg Radiol 8:293–296
Myerson SG (2012) Heart valve disease: investigation by cardiovascular magnetic resonance. J Cardiovasc Magn Reson 14(1):7
Nishimura RA et al (1997) Evaluation of diastolic filling of left ventricle in health and disease: Doppler echocardiography is the clinician's Rosetta Stone. J Am Coll Cardiol 30(1):8–18
Niwa K et al (2002) Progressive aortic root dilatation in adults late after repair of tetralogy of Fallot. Circulation 106:1374–1378
Nørgaard MA et al (2006) Major aorto-pulmonary collateral arteries of patients with pulmonary atresia and ventricular septal defect are dilated bronchial arteries. Eur J Cardiothorac Surg 29(5):653–658
Oosterhof T et al (2005) Corrected tetralogy of Fallot: delayed enhancement in right ventricular outflow tract. Radiology 237(3):868–871
Oosterhof T et al (2007) Preoperative thresholds for pulmonary valve replacement in patients with corrected tetralogy of Fallot using cardiovascular magnetic resonance. Circulation 116:545–551
Pacheco Duro R et al (2010) Anatomophysiologic basis of tetralogy of Fallot and its clinical implications. Rev Port Cardiol 29(04):591–630
Prieto LR (2005) Management of tetralogy of Fallot with pulmonary atresia. Images Paediatr Cardiol 7(3):24–42
Raman SV et al (2006) Multi-detector row cardiac computed tomography accurately quantifies right and left ventricular size and function compared with cardiac magnetic resonance. Am Heart J 151(3):736–744
Rebergen SA et al (1993) Pulmonary regurgitation in the late postoperative follow-up of tetralogy of Fallot. Volumetric quantitation by nuclear magnetic resonance velocity mapping. Circulation 88:2257–2266
Roes SD et al (2009) Flow assessment through four heart valves simultaneously using 3-dimensional 3-directional velocity-encoded magnetic resonance imaging with retrospective valve tracking in healthy volunteers and patients with valvular regurgitation. Investig Radiol 44(10):669–675
Saremi F et al (2013) Right ventricular outflow tract imaging with CT and MRI: part 1, morphology. Am J Roentgenol 200:W39–W50
Sharma A et al (2016) Ruptured aneurysm of major aortopulmonary collateral artery: management using amplatzer vascular plug. Cardiovasc Diagn Ther 6(3):274–277
Shimada YJ et al (2010) Accuracy of right ventricular volumes and function determined by three-dimensional echocardiography in comparison with magnetic resonance imaging: a meta-analysis study. J Am Soc Echocardiogr 23(9):943–953
Shimazaki Y et al (1984) The natural history of isolated congenital pulmonary valve incompetence: surgical implications. Thorac Cardiovasc Surg 32:257–259
Shinbane JS et al (2011) Magnetic resonance imaging in patients with cardiac pacemakers: era of "MR Conditional" designs. J Cardiovasc Magn Reson 13:63
Sommer RJ et al (2008) Pathophysiology of congenital heart disease in the adult. Part III: complex congenital heart disease. Circulation 117:1340–1350

Strait JB et al (2012) Aging-associated cardiovascular changes and their relationship to heart failure. Heart Fail Clin 8(1):143–164

Tharakan JA et al (2014) Post cardiac surgery junctional ectopic tachycardia: a 'Hit and Run' tachyarrhythmia as yet unchecked. Ann Pediatr Cardiol 7(1):25–28

Thierrien J et al (2000) Pulmonary valve replacement in adults late after repair of tetralogy of Fallot: are we operating too late? J Am Coll Cardiol 36(5):1670

Troughton RW et al (2014) Effect of B-type natriuretic peptide-guided treatment of chronic heart failure on total mortality and hospitalization: an individual patient meta-analysis. Eur Heart J 35(23):1559–1567

Valente AM et al (2014) Multimodality imaging guidelines for patients with repaired tetralogy of Fallot: A report from the American Society of Echocardiography. Developed in collaboration with the Society for Cardiovascular Magnetic Resonance and the Society for Pediatric Radiology. J Am Soc Echocardiogr 27:111–141

Vogel-Claussen J et al (2006) Delayed enhancement MR imaging: utility in myocardial assessment. Radiographics 26(3):795–810

Wald RM et al (2009) Effects of regional dysfunction and late gadolinium enhancement on global right ventricular function and exercise capacity in patients with repaired tetralogy of Fallot. Circulation 119(10):1370–1377

Wallerson DC et al (1987) Assessment of cardiac hemodynamics and valvular function by Doppler echocardiography. Bull N Y Acad Med 63(8):762–796

Warnes CA et al (2008) ACC/AHA 2008 guidelines for the management of adult with congenital heart disease: a report of the American College of Cardiology/American Heart Association Task Force on Practice Guidelines (Writing Committee to Develop Guidelines on the Management of Adults with Congenital Heart Disease). Circulation 118:e714–e833

Weber OM et al (2006) MR evaluation of cardiovascular physiology in congenital heart disease: flow and function. J Cardiovasc Magn Reson 8(4):607–617

Weisbord SD et al (2008) Incidence and outcomes of contrast-induced AKI following computed tomography. Clin J Am Soc Nephrol 3(5):1274–1281

Westhoff-Bleck M et al (2016) NT-proBNP indicates left ventricular impairment and adverse clinical outcome in patients with tetralogy of Fallot and pulmonary regurgitation. Can J Cardiol 32(10):1247.e29–1247.e36